

Photohadronic Neutrinos from Transients in Astrophysical Sources

Jörg P. Rachen and P. Mészáros

Department of Astronomy and Astrophysics, The Pennsylvania State University, University Park, PA 16802

e-mail: jrachen@astro.psu.edu, pmeszaros@astro.psu.edu

(Submitted: 17 February, 1998)

We investigate the spectrum of photohadronically produced neutrinos at very high energies (VHE, $\gtrsim 10^{14}$ eV) in astrophysical sources whose physical properties are constrained by their variability, in particular jets in Active Galactic Nuclei (blazars) and Gamma-Ray Bursts (GRB). We discuss in detail the various competing cooling processes for energetic protons, as well as the cooling of pions and muons in the hadronic cascade, which impose limits on both the efficiency of neutrino production and the maximum neutrino energy. If the proton acceleration process is of the Fermi type, we can derive a model independent upper limit on the neutrino energy from the observed properties of any cosmic transient, which depends only on the assumed total energy of the transient. For standard energetic constraints, we can rule out major contributions above 10^{19} eV from current models of both blazars and GRBs; and in most models much stronger limits apply in order to produce measurable neutrino fluxes. For GRBs, we show that the cooling of pions and muons in the hadronic cascade imposes the strongest limit on the neutrino energy, leading to cutoff energies of the electron and muon neutrino spectrum at the source differing by about one order of magnitude. We also discuss the relation of maximum cosmic ray energies to maximum neutrino energies and fluxes in GRBs, and find that the production of both the highest energy cosmic rays and observable neutrino fluxes can only be realized under extreme conditions; a test implication of this joint scenario would be the existence of strong fluxes of muon neutrinos up to energies $\gtrsim 10^{18}$ eV. Secondary particle cooling also leads to slightly revised estimates for the neutrino fluxes from (non-transient) AGN cores, which are commonly used in estimates for VHE detector event rates. Since our approach is quite general we conclude that the detection or non-detection of neutrinos above $\sim 10^{19}$ eV, e.g. with the Pierre Auger Observatory, correlated with blazar or GRB transients, would provide strong evidence against or in favor of current models for cosmic ray acceleration and neutrino production in these sources.

95.85.Ry, 98.54.Cm, 98.70.Sa, 98.70.Sz

I. INTRODUCTION

Neutrino astronomy may provide valuable clues for the understanding of the properties of neutrinos and their interactions at energies in the range $10^{14} - 10^{19}$ eV, as well as providing qualitatively new information about some of the most interesting cosmic objects. This energy range is also of great interest because it can probe the universe at significantly greater distances than is possible with known stellar sources (e.g. the Sun, or Supernovae such as 1987a, produce neutrinos in the \sim MeV range through nuclear interactions, which would be difficult to detect from more distant sources due to the overwhelming background of atmospheric neutrinos from cosmic ray air showers [1]). For these reasons, many of the future neutrino telescopes are designed for energies \gtrsim TeV, where the atmospheric background becomes negligible. Among the most promising and ubiquitous astrophysical sources of neutrinos at these very high energies are Active Galactic Nuclei and Gamma Ray Bursts [2], which have in common that most of their energetic emission appears in short, distinct flares. The study of the physical processes determining the energy spectrum of such neutrino emitting transients is the subject of this paper.

Above TeV energies and up to about 10^{17} eV neutrinos are detected predominantly through the Cherenkov effect in large volumes of water or ice, using the mass of the earth to capture neutrinos and looking for traces of upward going muons from $\nu_\mu \rightarrow \mu$ conversions; above 10^{17} eV air scintillation techniques and large air shower arrays become the most efficient to detect neutrino induced, deeply penetrating horizontal air showers, where electron neutrinos have the advantage to generate showers which are easier to distinguish from the cosmic ray background (see Appendix B for details and references). The major change of detection techniques at about 10^{17} eV motivates the distinction between very high energy (VHE) neutrinos at $10^{14}-10^{17}$ eV and ultra high energy (UHE) neutrinos at $\gtrsim 10^{17}$ eV. The most obvious source of UHE neutrinos are interactions of ultra-high energy cosmic rays with the universal microwave photon background, which predict a diffuse neutrino flux strong enough to be detected in air shower experiments [3]. More hypothetical is the prediction of UHE neutrinos from processes associated with grand unification scale physics, e.g. the annihilation topological defects [4]. In the VHE range, the major contribution is expected from Active Galactic Nuclei (AGN) [5-10], which are known to emit very high energy gamma rays. A possible contribution of AGN to the UHE neutrino regime is also discussed in connection with the expected event rates of horizontal air showers [11]. Also Gamma Ray Burst (GRB) sources have been proposed as neutrino sources in the MeV – GeV range [12], and at very high energies [13].

Neutrino production in hadronic models of AGN and GRB is generally attributed to the acceleration of protons in shocks or plasma turbulence, known as Fermi acceleration. These energetic protons then interact with soft background photons to produce pions (photohadronic pion production). VHE/UHE neutrinos originate in the decay of charged pions, boosted in energy by the original proton Lorentz factor, and maybe an additional Doppler factor due to the bulk motion of the rest frame of the relativistic outflows or jets which characterize these sources. The associated decay of neutral pions leads to the production of gamma rays, and it has been claimed that the observed emission up to $\gtrsim 10$ TeV in Doppler boosted AGN jets [14,15] is due to this process rather than inverse Compton scattering of photons by energetic electrons [16,17]. A relevant issue is that there are alternative models of AGN and GRB where the momentum and energy flux of the relativistic jets or outflows are provided by e^\pm or magnetic fields (e.g. [18,19] and references therein), rather than protons, and these would be expected to have negligible neutrino fluxes. The positive identification of VHE/UHE neutrinos from AGN and GRB would be a strong test for baryon loaded outflows. The energetic protons may also contribute to the highest energy cosmic ray spectrum, which is observed up to 3×10^{20} eV [20], where AGN and GRBs are considered among the most plausible sources. Here also, the observation or non-observation of energetic neutrinos would be a crucial test for these models.

The details of the photohadronic production of neutrinos via pion decay depend strongly on the properties of the source, i.e. its size, lifetime, magnetic field, etc. The magnitude of these quantities are estimated from the observed variability, flux, and the measured or inferred distance of these sources. GRB usually last $10^{-1} - 10^2$ seconds, but show intrinsic variability down to milliseconds, while AGN emit most of their energetic radiation in strong flares lasting several weeks, with intrinsic variability on time scales of days down to less than one hour. The transience of energetic emission could improve the association of detected neutrinos with their putative sources, because one could use both arrival direction and arrival time information, allowing statistically significant statements even for total fluxes below the background level.

On the other hand, transience and variability sets constraints on the maximum energy of the neutrino spectrum. In the literature so far, this has been connected to the maximum proton energy using simple kinematical relations. As we show in this paper, however, in these astrophysical scenarios the pions and muons in the photohadronic cascade have to be considered separately, since cooling processes can have a considerable impact on their final distribution. Moreover, one needs to evaluate carefully the competing proton energy loss processes that do not lead to neutrinos, which can cause breaks in the neutrino spectrum that are not present in the proton spectrum, and thus strongly limit the predicted fluxes at very high energies.

Starting with a general treatment of photohadronic neutrino production in variable sources, we derive a general upper limit for the maximum energy of neutrinos produced by photohadronic interactions of Fermi accelerated protons in cosmic transients, which only depends on the total energy of the transient and observational parameters, like duration or (photon) luminosity. We then apply our results to hadronic AGN and GRB models, and find that they impose severe constraints on their possible contribution to the UHE neutrino spectrum. Concerning notation, in what follows we always denote luminosities (\mathcal{L}) as being power per logarithmic interval of energy at a given energy. In Sect. III ff., calligraphic letters (e.g. \mathcal{L} , ε) denote quantities in the observer frame, whereas quantities in standard notation (e.g. L , ϵ) are in the comoving frame.

II. PHOTOHADRONIC NEUTRINO PRODUCTION

A. Proton cooling and neutrino production efficiency

Photohadronic neutrino production is a result of the decay of charged pions originating from interactions of high energy protons with ambient low energy photons. It is accompanied by the production of gamma rays from neutral pion decay; the details of the process are described in Appendix A, for a target photon spectrum following a power law with index a above a break energy ϵ_b . For the proton gas, pion production acts as a cooling process, and is in competition with other cooling processes like Bethe-Heitler pair production, synchrotron radiation, cosmic ray emission, and adiabatic losses due to the expansion of the emission region.

While neutrinos are exclusively produced by charged pion decay, gamma rays are produced by a variety of processes: besides neutral pion decay, $\pi^0 \rightarrow \gamma\gamma$, the major hadronically induced channels are synchrotron radiation from (a) the UHE protons themselves, (b) the electrons, muons and charged pions in the photohadronic decay chain (see Appendix A), and (c) the Bethe-Heitler pairs produced in $p\gamma \rightarrow pe^+e^-$ interactions [21]. If synchrotron cooling of pions and muons is negligible, about 25% of the energy lost in charged pions is converted into gamma radiation by synchrotron cooling of the electron produced in muon decay [22,16]. Normally, the first generation gamma rays cannot leave the emission region, but rather induce an electromagnetic cascade through pair production with low energy background photons, and subsequent synchrotron radiation of electrons and positrons. They cascade down in energy, until they eventually escape below some energy, ϵ_{esc} , where the emission region becomes optically thin [22]. Hadronically induced gamma rays are usually in competition with synchrotron and inverse Compton photons radiated by primary energetic electrons.

Cosmic rays can be ejected in essentially two ways: (a) if the emission region has a sharp border, beyond which the magnetic field drops rapidly, protons crossing this border can escape from the emission region, and (b) secondary neutrons produced in

$p\gamma$ interactions can escape if (1) their decay length, $\lambda_n = c\tau_n\gamma_n \gg R$, the size of the emission region, and (2) their probability of re-conversion to a proton by a reaction $n\gamma \rightarrow p\pi^-$ is small, expressible by $ct_{n\rightarrow p} \gg R$. Process (a) depends on the detailed structure of the emission region and is usually in competition with adiabatic cooling, which affects charged particles due to the adiabatic invariance of the quantity Br_L^2 during the Larmor motion of the particle ($r_L = E/eB$ is the Larmor radius) in a magnetic field decreasing with expansion [23]. In an isotropically expanding emitter with conserved total magnetic energy this means $B \propto R^{-2}$, and thus $E \propto R^{-1}$, but other dependences may apply (see Sect. III B 1). Process (b) is tightly connected to neutrino production, because the dominant channel producing charged pions, $p\gamma \rightarrow n\pi^+$, is also the dominant channel for neutron production. The time scale for proton-neutron conversion is $t_{p\rightarrow n} \approx t_{n\rightarrow p} \approx 2t_{p,\pi}$, which is larger than the time scale for charged pion production, $t_{\pi^\pm} \approx \frac{3}{2}t_{p,\pi}$ (Appendix A), because there the process $p\gamma \rightarrow p\pi^+\pi^-$ contributes considerably.

Neutrino production is efficient if (i) the protons convert a considerable fraction of their energy into charged pions, and (ii) the pions and muons keep most of their energy until they decay. Condition (ii) can be quantified by introducing the efficiency of energy conversion from the originally produced pion into neutrinos, $\zeta_{\nu,\mu}^{\text{dc}} = \frac{1}{2}(\gamma_\mu^{\text{dc}}/\gamma_\pi^{\text{pr}})$ and $\zeta_{\nu,\pi}^{\text{dc}} = \frac{1}{4}(\gamma_\pi^{\text{dc}}/\gamma_\pi^{\text{pr}})$, for muon and pion decay, respectively. Similarly we can quantify (i) by introducing the charged pion production efficiency, $\zeta_{\pi^\pm} = \bar{t}_p/t_{\pi^\pm}$, where \bar{t}_p is the total cooling time of the proton. This leads to the total neutrino production efficiency

$$\zeta_\nu(\gamma_p) = \zeta_{\pi^\pm}(\zeta_{\nu,\pi}^{\text{dc}} + \zeta_{\nu,\mu}^{\text{dc}}) \approx \left(\frac{1}{3} \frac{\gamma_\mu^{\text{dc}}}{\gamma_p} + \frac{1}{6} \frac{\gamma_\pi^{\text{dc}}}{\gamma_p} \right) \frac{\bar{t}_p}{t_{p,\pi}} \quad (1)$$

where we used $\gamma_\pi^{\text{pr}} \approx \gamma_p$ and $t_{\pi^\pm} \approx \frac{3}{2}t_{p,\pi}$. The total proton cooling time is determined by the inverse sum, $\bar{t}_p^{-1} = \sum_i t_{p,i}^{-1}$, extending over all participating cooling processes.

To classify the cooling processes by their dependence on γ_p , we introduce total cooling times for photohadronic interactions, $t_{p\gamma}$, synchrotron radiation, $t_{p,\text{syn}}$, and external cooling processes, t_{ec} . Under external cooling processes we subsume adiabatic cooling, which has a time scale t_{ad} independent of the proton energy, and direct ejection of protons from the emission region. The latter may be dependent on the proton energy if diffusive losses are relevant; in the simplest case, however, we can assume that protons are confined over the time scale set by adiabatic expansion, i.e. $t_{\text{esc},p} \gg t_{\text{ad}}$, which means that

$$t_{\text{ec}} \simeq t_{\text{ad}} = \text{const}(\gamma_p) \quad . \quad (2)$$

The synchrotron loss time can be written as

$$t_{p,\text{syn}} = t_{\text{b,syn}} \left(\frac{\gamma_p}{\gamma_b} \right)^{-1} \quad \text{with} \quad t_{\text{b,syn}} = \frac{9c}{4r_p \omega_{B,p}^2 \gamma_b} , \quad (3)$$

where $r_p = e^2/m_p c^2 \approx 1.5 \times 10^{-16}$ cm is the classical proton radius, and $\omega_{B,p} = eB/m_p c \sim [10^4 \text{ s}^{-1}] B_G$ is the cyclotron frequency of the proton with B_G being the magnetic field strength in gauss. The characteristic proton Lorentz factor used here for normalization,

$$\gamma_b \equiv \epsilon_{\text{th}}^{\text{RF}}/2\epsilon_b \quad (4)$$

expresses the limit above which all photons in the power law part of the spectrum are boosted above the reaction threshold for pion production (see Appendix A).

Assuming that the photon number spectrum can be described as a power law, $dN_{\text{ph}} \propto \epsilon^{-a} d\epsilon$, with an index $a > 1$ above some break energy ϵ_b (see Appendix A for details), the cooling due to both charged and neutral pion production can be written as a function of γ_p as

$$t_{p,\pi} = t_{\text{b},\pi}(\gamma_p/\gamma_b)^{1-a} \quad \text{for} \quad \gamma_p < \gamma_b \quad (5a)$$

$$t_{p,\pi} \approx t_{\text{b},\pi}(N_{\text{ph},b}/N_{\text{ph}}) \quad \text{for} \quad \gamma_p \gg \gamma_b , \quad (5b)$$

where N_{ph} is the total photon density, $N_{\text{ph},b}$ is the density of photons with $\epsilon > \epsilon_b$. $t_{\text{b},\pi}$ is the pion production cooling time for protons with $\gamma_p = \gamma_b$, and can be expressed as $t_{\text{b},\pi} \simeq [cN_{\text{ph},b}H_a]^{-1}$, where H_a is the inelasticity weighted effective cross section for pion production, as defined in Appendix A.

The time scales for other photohadronic cooling processes, including neutron ejection, can all be expressed in $t_{p,\pi}$. The cooling time for the Bethe-Heitler process can be evaluated similarly to Eqs. (5) and (A2); the inelasticity weighted cross section for the Bethe-Heitler process is $H_a^{\text{BH}} \approx H_a/125$, for a break Lorentz factor $\gamma_{b,\text{BH}} \approx \gamma_b/140$, leading to $f_{\text{BH}} \equiv t_{p,\pi}/t_{p,\text{BH}} \approx \exp(5a - 10)$ for $\gamma_p \lesssim \gamma_{b,\text{BH}}$, and $f_{\text{BH}} \ll 1$ for $\gamma_p \gg \gamma_{b,\text{BH}}$. To quantify the time scale for energy loss due to free neutron escape, $t_{\text{esc},n}$, we introduce the probabilities for neutron-to-proton reconversion within the length scale of the emission region R , due to beta decay, $P_{n\beta} = \exp(-\lambda_n/R)$, and due to pion production, $P_{n\gamma\rightarrow p} \approx \exp(-2ct_{p,\pi}/R)$, using $t_{n\rightarrow p} \approx 2t_{p,\pi}$. Since the typical energy ratio of the neutron to the pion in a $p\gamma \rightarrow n\pi^+$ reaction is ≈ 4 , we finally get $t_{\text{esc},n} \approx \frac{1}{2}P_{\text{esc},n}^{-1}t_{p,\pi}$, where

$P_{\text{esc},n} = (1 - P_{n\gamma \rightarrow p})(1 - P_{n\beta})$ is the probability of the neutron to escape. With $t_{p\gamma}^{-1} \equiv t_{p,\pi}^{-1} + t_{\text{esc},n}^{-1} + t_{p,\text{BH}}^{-1}$, and using the fact that beta decay and photohadronic interactions for neutrons are likely in different Lorentz factor regimes, i.e. $P_{n\beta}P_{n\gamma \rightarrow p} \ll 1$, we can write

$$f_{p\gamma} \equiv \frac{t_{p,\pi}}{t_{p\gamma}} \approx 3 + \exp(5a - 10) - 2 \exp\left(-\frac{c\tau_n\gamma_p}{R}\right) - 2 \exp\left(-\frac{2ct_{p,\pi}}{R}\right) \quad (6)$$

for $\gamma_p \lesssim 0.01\gamma_b$. For $\gamma_p \gtrsim \gamma_b$, the term expressing the Bethe-Heitler efficiency, $\exp(5a - 10)$, is absent. Assuming $t_{\text{ec}} \approx t_{\text{ad}}$ we can write

$$\frac{t_{p,\pi}}{t_p} = t_{p,\pi} \left(t_{p\gamma}^{-1} + t_{\text{syn}}^{-1} + t_{\text{ec}}^{-1} \right) \approx \max(f_{\text{ad}}, f_{p\gamma}, f_{\text{syn}}) \equiv f_{\text{max}}, \quad (7)$$

where $f_{\text{syn}} \equiv t_{p,\pi}/t_{\text{syn}}$ and $f_{\text{ad}} \equiv t_{p,\pi}/t_{\text{ad}}$ are defined analogously to $f_{p\gamma}$, i.e. expressing the energy dissipated in the various cooling channels in units of the energy lost in pion production. The approximation by the maximum-function is best if one cooling process clearly dominates; it is useful for the following, qualitative discussion of the shape the time integrated neutrino spectrum.

B. Shape of the time integrated neutrino spectrum

Because of the low detection efficiency of neutrinos at earth, it is impossible with present techniques to observe short scale time variability of cosmic neutrino spectra. Therefore, for an outburst active over a limited time, it is more meaningful to calculate the time integrated neutrino count spectrum, rather than the spectral count rate at a fixed time. This also simplifies the theoretical treatment, because we do not need to perform a self consistent calculation of the accumulated proton spectrum at a specific time — the energy input at any specific energy is simply given by the time integrated proton *injection* spectrum.

Clearly, the proton spectrum injected by the acceleration process is not directly observable. We will follow here the scenario assumed in most models, i.e. that the average injection rate for energetic protons follows a power law in energy, $\langle d\dot{N}_p \rangle = I_p \gamma_p^{-s} d\gamma_p$, extending from some minimum Lorentz factor $\tilde{\gamma}_p \sim 1$ to a maximum Lorentz factor $\hat{\gamma}_p \gg 1$. We assume that the injection is active over a time T_{inj} , and that the injection spectrum does not change in time. Then the total, time integrated energy density of injected protons is given by

$$\bar{u}_p = T_{\text{inj}} \int_{\tilde{\gamma}_p}^{\hat{\gamma}_p} m_p c^2 \gamma_p \langle d\dot{N}_p \rangle d\gamma_p = A_s m_p c^2 T_{\text{inj}} I_p, \quad (8)$$

where the normalization constant can be approximated by $A_s \approx \hat{\gamma}_p^{2-s}/(2-s)$ for $s < 2$, $A_s \approx \ln(\hat{\gamma}_p/\tilde{\gamma}_p)$ for $s \simeq 2$, and $A_s \approx \tilde{\gamma}_p^{2-s}/(s-2)$ for $s > 2$.

Protons injected at a specific Lorentz factor γ_p produce charged pions with $\gamma_{\pi}^{\text{pr}} \approx \gamma_p$ at a rate $t_{\pi\pm}^{-1}$, over a time \bar{t}_p . Thus, the total number density of charged pions produced in the emission process is $dN_{\pi} = T_{\text{inj}} \langle d\dot{N}_p \rangle \bar{t}_p t_{p,\pi}^{-1}$. Each charged pion produces two muon neutrinos ($\nu_{\mu}\bar{\nu}_{\mu}$) and one electron neutrino (ν_e or $\bar{\nu}_e$), each with an energy $E_{\nu} \simeq \frac{1}{4}m_{\pi}c^2\gamma_p$ if we assume that $\gamma_{\mu}^{\text{dc}} \approx \gamma_{\pi}^{\text{dc}} \approx \gamma_p$. Then, the total time integrated neutrino power at the energy E_{ν} emitted by the source in its rest frame is

$$\bar{L}_{\nu}(E_{\nu}) \equiv E_{\nu} \frac{dN_{\nu}}{d\ln E_{\nu}} = \frac{V\bar{u}_p}{A_s} \Phi\left(\frac{4E_{\nu}}{m_{\pi}c^2}\right), \quad (9)$$

where V is the volume of the emission region. The spectral shape is expressed by the function $\Phi(\gamma_p) = \gamma_p^{2-s}\zeta_{\nu}(\gamma_p)$, which can be written as $\Phi(\gamma_p) = \gamma_p^{2-s}f_{\text{max}}^{-1}(\gamma_p) \propto \gamma_p^q$ in the case of one dominating cooling process; the power law index q is, depending on the dominant cooling process, given by

regime	:	$\gamma \lesssim \gamma_b$	$\gamma \gg \gamma_b$
$f_{\text{max}} = f_{\text{ad}}$:	$q = a - s + 1$	$q = 2 - s$
$f_{\text{max}} = f_{p\gamma}$:	$q = 2 - s$	$q = 2 - s$
$f_{\text{max}} = f_{\text{syn}}$:	$q = a - s$	$q = 1 - s$

where a is the target photon spectral index. For $a > 2$, an additional spectral modification will occur due to the drop of the Bethe-Heitler efficiency between $\sim 0.01\gamma_b$ and $\sim \gamma_b$, if photohadronic cooling is dominant in this region (i.e. $f_{\text{max}} = f_{p\gamma}$); in this case, one would expect a rapid rise in the neutrino flux in the regime $E_{\nu} \lesssim [30 \text{ MeV}] \gamma_b$.

The energy dependence of neutrino event rate as observed in a given detector follows closely the neutrino power spectrum, as shown in Appendix B, if we properly account for energy shifts due to Doppler boosting or source redshift. In general, we will expect an increase of events with energy for $q > 0$, a decrease for $q < 0$, and $q \approx 0$ would indicate an event rate almost independent of energy. If the proton spectral index is close to the canonical value for shock acceleration, $s \approx 2$, we would therefore expect a “flat” event rate if $q = 2 - s$; this is the case if photohadronic cooling dominates, or for synchrotron dominated cooling in case of $\gamma < \gamma_b$ and a flat background photon spectrum, $a \approx 2$. If adiabatic cooling is the dominant process, however, the neutrino spectrum is flatter than the proton spectrum, and the event rate would increase with energy. In the general case, we expect a “plateau-like” neutrino event rate, i.e. increasing up to some break energy, and then approximately constant up to the cutoff, which can be most easily understood as a saturation effect: for small Lorentz factors, the efficiency for pion production (relative to adiabatic cooling) increases, until it eventually reaches a maximum determined by the ratio of photohadronic and synchrotron cooling times. Above the characteristic Lorentz factor, γ_b , associated to the break in the photon spectrum at ϵ_b , the neutrino spectrum also has the same spectral index as the injected protons, unless synchrotron cooling dominates, where the neutrino spectrum is steeper by one power because the photohadronic efficiency decreases with $t_{\text{syn}}/t_{p\gamma} \propto \gamma_p^{-1}$. A more illustrative discussion is given for the special cases of AGN jets and GRBs in Sect. IV.

III. NEUTRINO EMISSION FROM COSMIC TRANSIENTS: GENERAL THEORY

Neutrino bursts themselves may only be observable in their time integrated appearance. However, the accompanying burst of photons is observable in much greater detail, and allows to constrain the physical parameters determining neutrino production. We have to distinguish between low energy photons, which are in general explained by synchrotron radiation of electrons co-accelerated with the protons, and high energy gamma radiation, which may be dominated by hadronically induced cascades, as discussed above, but could also originate dominantly from inverse Compton photons produced by the electrons.¹ The following discussion is more focussed on the low energy photon component, which is relevant as the target population for photohadronic neutrino production. However, if the high energy photons are of hadronic origin, their variability can also give valuable clues on proton cooling times.

Hereafter, we will distinguish between physical quantities defined in the comoving frame of the source (denoted with standard letters, e.g. E , T , L , etc.), and observed quantities (denoted with calligraphic letters, e.g. \mathcal{E} , \mathcal{T} , \mathcal{L} , etc.), where we account for a possible boosting of the radiation emitted from the source with a Doppler factor \mathcal{D} , given by

$$\mathcal{D} = \left[\Gamma(1 - \beta_\Gamma \cos \Theta_{\text{view}}) \right]^{-1} \quad \text{with} \quad \beta_\Gamma = \sqrt{1 - \Gamma^{-2}}, \quad (10)$$

for a relativistic flow with Lorentz factor Γ and a velocity $\beta_\Gamma c$ under an angle Θ_{view} to the direction of the observer. We will not take into account redshift effects, and just note that they might be considered by replacing $\mathcal{D} = \mathcal{D}'/(1+z)$, if \mathcal{D}' is the Doppler factor of the emission region in the cosmologically comoving frame at the source. The task will be to constrain the physical properties of the emission region by observable quantities, in order to discuss the various processes limiting the neutrino energy. Each process can be assigned a specific critical neutrino energy in the observers frame, $\hat{\mathcal{E}}_{\nu, \text{proc}}$, above which the neutrino spectrum steepens. We discuss a meaningful choice for the “cutoff energy” of the neutrino spectrum, $\hat{\mathcal{E}}_\nu$, at the end of the section.

A. Variability time scales and the size of the emission region

1. The causality limit

If a flare occurring in a relativistic outflow, boosted with a Doppler factor \mathcal{D} , is observed to have a duration \mathcal{T} , the time scale of the burst in the comoving frame of the fluid is $T = \mathcal{T}\mathcal{D}$. This “intrinsic” time scale covers (a) the time scale for the injection of energetic particles, T_{inj} , (b) the time scale over which the particles convert their energy in radiation, T_{rad} , and (c) the crossing time the photons need to leave the emission region, T_{cr} . These partial times involved in the outburst normally do not simply add up; by order of magnitude, however, it may be appropriate to write

$$T \sim \max(T_{\text{inj}}, T_{\text{rad}}, T_{\text{cr}}) \quad . \quad (11)$$

¹The terms “low energy” and “high energy” are here used only in a meaning relative to each other. The absolute energy range for electron synchrotron radiation on the one hand, and electron Compton radiation or PIC photons on the other, depends strongly on the physical conditions at the source. Energy ranges are, for instance, very different in AGN compared to GRBs.

The crossing time is naturally connected to the (comoving) linear size of the emission region, $R = cT_{\text{cr}}$. If the emission region is not spherically symmetric, we can only limit the comoving size along the line of sight, R_{\parallel} , by the observed duration as

$$R_{\parallel} = cT_{\text{cr}\parallel} = c\rho_T T \mathcal{D} \quad , \quad (12)$$

where the factor $\rho_T \leq 1$ considers the effect of a delayed emission due to finite injection or radiation time scales; $\rho_T = 1$ means that the emission is homogeneous and instantaneous within the size R — the observed duration is then simply the time between the first and the last photon reaching us. Since the condition $T \geq T_{\text{cr}}$ is equivalent to the requirement that the emission throughout the emission region is due to one, causally connected process, Eq. (12) may be called the *causality limit* for the size of transient source.

The projected (or lateral) comoving size, R_{\perp} , is not constrained by the variability time scale, but plays a role for the determination of the internal radiation density of the emission region from its observed, isotropized luminosity at a specific photon energy, $\mathcal{L}(\epsilon) = 4\pi d_L^2 \epsilon^2 (dN_{\text{ph}}/d\epsilon)_{\text{obs}} = \mathcal{D}^4 L(\epsilon)$ with $\epsilon = \mathcal{D}\epsilon$, where d_L is the luminosity distance of the source (note that the redshift is absorbed in the Doppler factor, as explained above). To account for this, we introduce a geometrical eccentricity parameter, x_L , by writing the luminosity as

$$L(\epsilon) = 4\pi R_{\parallel}^2 c x_L \epsilon^2 (dN_{\text{ph}}/d\epsilon) \quad , \quad (13)$$

where $\epsilon^2 (dN_{\text{ph}}/d\epsilon)$ is the specific energy density of photons with energy ϵ in the rest frame of the flow. For a spherically symmetric emission region $x_L = 1$, while a disk like emission region with $R_{\parallel} \ll R_{\perp}$ could be described with $x_L \sim (R_{\perp}/R_{\parallel})^2 \gg 1$.

The radiation time scale is obviously equivalent to the cooling time scale of the radiating particles; for radiation processes involving electrons, it is usually very short, $T_{\text{rad}} \ll T_{\text{cr}}$, justifying its neglect. If we consider radiation produced in photohadronic interactions, we can write $T_{\text{rad}} \approx \bar{t}_p$, since the time scale over which the electromagnetic cascade evolves can be considered as short compared to \bar{t}_p . T_{inj} is the time over which an acceleration process is active, e.g. the lifetime of a shock. Obviously, this sets a limit on the acceleration time of the particles, $t_{\text{acc}} < T_{\text{inj}} < T\mathcal{D}$. Also here, this is barely relevant for electrons, but sets an important limit for protons.

2. The internal shock scenario

As an example how observed time scales in transient emission phenomena may be connected to the size of the emission region, we discuss the scenario of energy conversion in relativistic flows by internal shocks. This scenario was suggested originally by Rees [24] for AGN jets, and was later also applied to Gamma Ray Bursts [25].

We consider two plasma blobs of similar mass and density emitted within an unsteady flow at times t_1 and t_2 , $\Delta t = t_2 - t_1 > 0$, with respective Lorentz factors Γ_1 and Γ_2 , $\Gamma_2/\Gamma_1 \gtrsim 1$, i.e. the second blob has a larger velocity and thus catches up with the first after some time $\sim \Gamma_1 \Gamma_2 \Delta t$. Assuming that their relative velocities are supersonic, two strong shock waves moving in opposite directions form when the blobs merge; they are called *forward shock* and *reverse shock*, respective to their direction of motion relative to the flow. In their center of mass frame (CMF), which has a Lorentz factor $\Gamma \simeq \sqrt{\Gamma_1 \Gamma_2}$ in the observers frame, the shocked material in region between the two shocks is at rest, and is the source of the radiation. The shocks move each with a velocity $\beta_{\text{sh}} c$, $\beta_{\text{sh}} \approx \sqrt{1 - \Gamma_1/\Gamma_2}$, corresponding to a internal shock Lorentz factor $\Gamma_{\text{sh}} \approx \sqrt{\Gamma_2/\Gamma_1}$. The linear size of the emitter in the direction of the flow, after the merging is complete, is $R_{\parallel} = 2R'_{\parallel}/\chi$, if R'_{\parallel} is the length of the blobs in this direction in their respective rest frames, and $\chi = 4\Delta\Gamma + 3$ is the compression factor. Therefore, $T_{\text{inj}} \approx R'_{\parallel} \chi / \beta_{\text{sh}} = T_{\text{cr}}/2\beta_{\text{sh}}$, the time each shock needs to cross half this distance. For transrelativistic internal shocks, $\beta_{\text{sh}} \sim \frac{1}{2}$, the crossing time is therefore a good measure for the injection time scale. The total efficiency for the dissipation of energy by the shocks is given by $\xi_{\text{sh}} = 1 - 2\Gamma_{\text{sh}}/(1 + \Gamma_{\text{sh}}^2)$, and is about 20% for $\Gamma_{\text{sh}} \approx 2$.

We now assume that the radiation time scale is much shorter than the dynamic time scales involved in the shock merging. Then, the emission follows closely the motion of the shocks; if the observer is positioned in an angle $\Theta_{\text{view}} \ll 1$ to the flow direction, the emission of the forward shock appears in the observer frame as a peak of duration $T_f = T_{\text{inj}} \mathcal{D}^{-1} (1 - \beta_{\text{sh}})$, while the emission of the reverse shock causes a peak with a duration $T_r = T_{\text{inj}} \mathcal{D}^{-1} (1 + \beta_{\text{sh}})$, and comparable total energy. For $\beta_{\text{sh}} \sim \frac{1}{2}$, the two peaks can thus have different lengths (but of the same order of magnitude), and the total, superposed peak might appear asymmetric, with a rise time $T_{\uparrow} \approx T_f/2\mathcal{D}$, and a decay time $T_{\downarrow} \approx (T_r - \frac{1}{2}T_f)\mathcal{D}^{-1}$. The crossing time is then correctly estimated by $T_{\text{cr}} = T\mathcal{D}$ (or $\rho_T = 1$), if we define

$$T \equiv T_r - T_f \approx T_{\downarrow} - T_{\uparrow} \quad . \quad (14)$$

We stress that this result is *independent of β_{sh}* .

Eq. (14) makes use of several assumptions: (a) that the two plasma blobs have comparable densities, and (b) that $T_{\text{rad}} \ll T_{\text{cr}}$. Condition (b) is mostly fulfilled, if we consider synchrotron of inverse radiation from energetic electrons. Condition (a) can be

assumed to nearly fulfilled in internal shocks — which is the most important difference to *external* shocks, where the densities are usually very different. If (a) is not fulfilled, forward and reverse shock have different velocities in the CMF, and also different efficiencies in energy conversion [26,27]: hence, the forward and backward peak have very different strengths, and the correlation of T_f and T_r with T_\uparrow and T_\downarrow is less straightforward. If (b) is not fulfilled, i.e. if $T_{\text{rad}} > T_{\text{cr}}$, we expect $T_{\text{rad}} \sim T_\uparrow \mathcal{D}$, and $T_{\text{cr}} \sim T_\uparrow \mathcal{D}$. A similar situation arises for fast cooling, but the presence of a secondary acceleration process which is not associated to the shock waves (e.g. second order Fermi acceleration, see Appendix C), which can keep up a population of energetic particles homogeneously over the region of the shocked gas, and thus extend the emission as in the case of slow cooling.

In summary, we see that there is no “foolproof instruction” how to “read” the shape of an observed radiation flare, in order to estimate the crossing time correctly. However, for flares with considerable asymmetry, $T_\downarrow - T_\uparrow \sim T_\downarrow$, Eq.(14) can be assumed to guarantee $\rho_T \leq 1$, thus give an upper limit on the crossing time. We also note that the geometrical eccentricity parameter, x_L , as introduced in Eq. (13), satisfies the relation $x_L = \chi^2 x'_L$, if x'_L is the eccentricity of the blobs before they merge. Since $\chi^2 \gtrsim 10$ for transrelativistic shocks, this may give rise to assume rather disk-like geometries in the internal shock scenario; this conclusion, however, may not be over-interpreted because we can obviously not rule out that the blobs have been originally elongated in the flow direction, i.e. $x'_L < 1$. The internal shock mechanism can readily be applied to spherical (or quasi-spherical) outbursts, where the up-catching “blobs” have to be replaced by shells emitted with different velocities at different times [25]. We discuss this scenario, and its implication for the geometrical factors ρ_T and x_L , in more detail in Sect. IV B 1.

B. Maximum energy of accelerated protons

The predominance of power laws in nonthermal emission spectra suggests that the radiating particles gain their energy by a stochastic process. Based on an original idea of Fermi [28], the most commonly discussed stochastic acceleration processes fall into two parts: (a) *first order Fermi-acceleration* by diffusive scattering of particles across strong shock waves, also called *shock-acceleration* [29] and (b) *second order Fermi-acceleration*, where the particles gain energy from the scattering at plasma waves [30,31]. Since plasma waves are responsible for the scattering, and thus for the diffusive motion of particles in shock acceleration as well, it is most likely that both processes combine if strong shock waves are present [32]. Fermi acceleration is assumed to be the dominant energy dissipation mechanism in AGN cores and jets, and in Gamma Ray Bursts. Since Fermi acceleration works independent of particle mass and charge, any protons or ions present at the shock should be accelerated as well as electrons. It has been claimed for various classes of objects that this could be the generating process of the observed cosmic ray spectrum, up to the highest energies of order 10^{20} eV [20].

In the following we discuss the maximum energies of protons Fermi-accelerated in emission regions constrained by variability. The time scale for Fermi acceleration will be expressed as a multiple of the Larmor time of the particle, $t_{\text{acc}} \equiv \theta_F t_L = 2\pi \theta_F r_L / c$. The value of the constant θ_F is discussed in more detail in Appendix C, where we point out that $\theta_F \gg 1$ applies in the general case, but $\theta_F \sim 1$ is probably possible for acceleration at relativistic shocks.

1. Larmor radius and adiabatic limits

For protons to be accelerated up to an energy \hat{E}_p by a Fermi mechanism, we have to require that the proton can be magnetically confined in the emission region, i.e. $E_p < eBR_{\min}$, $R_{\min} = \min(R_{\parallel}, R_{\perp})$. Using the relations $R_{\parallel} < c\mathcal{T}\mathcal{D}$, $E_\nu \leq \frac{1}{4}m_\pi c^2 \gamma_p$, and $\mathcal{E}_\nu = E_\nu \mathcal{D}$, we can write

$$\hat{\mathcal{E}}_{\nu, L(p)} = \frac{em_\pi c}{4m_p} B T \mathcal{D}^2 \rho_T \rho_L \quad (15a)$$

The factor $\rho_L < 1$ considers that usually only a limited fraction of the effective size R_{\min} of the emission region can practically be used for particle gyration; we will assume $\rho_L \lesssim \frac{1}{3}$ in the following.

Similar limits can be derived from acceleration time constraints arising from the dynamic time scales involved in the acceleration process. The first condition of this kind is $t_{\text{acc}} < T_{\text{inj}}$, which can be specified in the internal shock scenario as $t_L < T_{\text{cr}}/2\theta_F \beta_{\text{sh}}$, is obviously equivalent to Eq.(15a) with $\rho_L = (2\theta_F \beta_{\text{sh}})^{-1}$. The second condition is the limitation of the acceleration time by adiabatic cooling in a decreasing magnetic field, $t_{\text{acc}} < t_{\text{ad}} \equiv 2B/\dot{B}$. In an expanding emission region, we usually find $B \propto R^{-\alpha}$, where $\alpha > 0$ and R is some characteristic size of the emission region. In the general case, in particular for non-isotropic expansion, α may depend on the choice of R ; in an isotropically expanding emitter with conserved magnetic energy we have $\alpha = 2$, which we may use as a canonical assumption hereafter. Defining the velocity of expansion as $\beta_{\text{ex}} \equiv \dot{R}/c$, this results again in Eq.(15a), with $\rho_L = (\pi\alpha\theta_F \beta_{\text{ex}})^{-1}$. Adiabatic cooling is most relevant in a freely expanding relativistic fluid, $\beta_{\text{ex}} \approx 1$, or for rapidly decaying magnetic fields, $\alpha \gg 1$ (however, we have to assume that the field decay is adiabatic, i.e. $B/\dot{B} \gg t_L$), while it is less relevant in magnetically confined flows ($\alpha\beta_{\text{ex}} \ll 1$). For second order Fermi

acceleration, both constraints, $t_{\text{acc}} < T_{\text{inj}}$ and $t_{\text{acc}} < t_{\text{ad}}$, are equivalent, because the injection time is limited by the adiabatic drop of the Alfvén speed, which leads to $T_{\text{inj}} \sim t_{\text{ad}}$.

In conclusion, Eq. (15a) with $\rho_L \sim \min(\frac{1}{3}, \theta_F^{-1})$ applies as an upper limit for our canonical assumption that either $\beta_{\text{ex}} \gtrsim \frac{1}{3}$ or $\beta_{\text{sh}} \gtrsim \frac{1}{2}$, i.e. that the involved hydrodynamic process are at least transrelativistic. Acceleration time constraints then dominate for $\theta_F > 1$, which is particularly the case for second order Fermi acceleration, or acceleration at nonrelativistic, quasi-parallel shocks (c.f. Appendix C), while for any faster acceleration mechanism the geometrical extension of the emission region, constrained by variability, sets the limit on \mathcal{E}_ν .

2. Limits due to radiative cooling

Synchrotron cooling of the protons during acceleration limits their maximum energy through the condition $t_{\text{acc}} < t_{p,\text{syn}}$. Writing the acceleration time as $t_{\text{acc}} = 2\pi\theta_F\gamma_p/\omega_{B,p}$ and using Eq. (3), we find $\gamma_p < 3/\sqrt{8\pi\theta_F r_p \omega_{B,p}}$, leading to

$$\hat{\mathcal{E}}_{\nu,\text{syn}(p)} \approx \frac{3}{20} \frac{m_\pi c^2 \mathcal{D}}{r_p} \sqrt{\frac{e}{\theta_F B}} \quad . \quad (15b)$$

In the same way, proton acceleration must be faster than the cooling due to photohadronic interactions, $t_{\text{acc}} < t_{p\gamma} \approx f_{p\gamma}^{-1} t_{p,\pi}$. To express $t_{b,\pi}$ by observable quantities, we use Eq. (13) to write

$$t_{b,\pi} = \frac{4\pi\mathcal{D}^5 T^2 \rho_T^2}{T_c} \quad \text{with} \quad T_c = \frac{\mathcal{L}_b H_2}{c^2 \varepsilon_b x_L (a-1)^2} \quad (16)$$

where $\mathcal{L}_b \equiv \mathcal{L}(\varepsilon_b)$ is the isotropic luminosity of the source at the observed spectral break, related to the break energy in the comoving frame by $\varepsilon_b = \epsilon_b \mathcal{D}$, and $H_2 \approx 22 \mu\text{barn}$ (c.f. Appendix A). Using Eqs. (5) we obtain from $t_{\text{acc}} < t_{p\gamma}$

$$\hat{\mathcal{E}}_{\nu,p\gamma} \lesssim \frac{m_\pi c^2 \tilde{\gamma}_b}{4} \left[\frac{3\omega_{B,p} T \rho_T}{2\pi\theta_F f_{p\gamma} \Upsilon_1 \tilde{\gamma}_b} \right]^{\frac{1}{a}} \mathcal{D}^{2+4/a} \quad \text{for} \quad \frac{2\omega_{B,p} T^2 \rho_T^2 \mathcal{D}^4}{\theta_F f_{p\gamma} T_c} \lesssim \tilde{\gamma}_b \quad (17)$$

where we inserted the Doppler scaled characteristic Lorentz factor, $\tilde{\gamma}_b = \epsilon_{\text{th}}^{\text{RF}}/2\varepsilon_b$, which does not depend on \mathcal{D} and is related to the comoving characteristic Lorentz factor by $\gamma_b = \tilde{\gamma}_b \mathcal{D}$, and

$$\Upsilon_1 = \begin{cases} 3T_c/4\pi T \rho_T & \text{for } \hat{\gamma}_p \lesssim \gamma_b \\ 3T_c N_{\text{ph}}/4\pi N_{\text{ph,b}} T \rho_T & \text{for } \hat{\gamma}_p \gg \gamma_b \end{cases} \quad . \quad (18)$$

The case of Eq. (17) obviously corresponds to $\hat{\gamma}_p \lesssim \gamma_b$; the case $\hat{\gamma}_p \gg \gamma_b$ is described by setting $a = 1$ and using the proper value for Υ_1 . It should be noted that Eq. (17) only considers the photon density in the burst connected to its intrinsic luminosity. If, however, the relativistically moving ‘‘blob’’ is embedded in an ambient photon field, which is isotropic with respect to the observer, the photon density seen in the comoving frame of the blob can be considerably higher than inferred from the observed luminosity by Eq. (13). The reason is, that this additional component would appear unboosted for the observer, and therefore probably only as a small fraction of the apparent luminosity of the emitting blob, which is boosted by a factor \mathcal{D}^4 . In contrast, in the comoving frame the photon number density of the ambient component is further increased by a factor \mathcal{D} due to Lorentz contraction, and may dominate over the intrinsic photon density. This scenario might be relevant in AGN, if the emission region in the jet is close to the AGN core, and if the core radiation is isotropized by a plasma halo (see, e.g. [33]). Thus, the maximum neutrino energy constrained through photohadronic interactions may be considerably below the upper limit expressed by Eq. (17).

C. Cooling of pions and muons in the hadronic cascade

1. Cooling processes and time scales

Pions and muons are weakly decaying particles, with comparatively long lifetimes, $\tau_\pi = 2.6 \times 10^{-8} \text{ s}$ and $\tau_\mu = 2.2 \times 10^{-6} \text{ s}$, respectively. For Lorentz factors² $\gamma_*^{\text{pr}} \approx \gamma_p \gtrsim 10^{6-8}$, which are quite reasonable and readily considered in most models,

²We symbolize unstable particles in the hadronic cascade, i.e. pions and muons, by ‘‘*’’, if they are not specified.

their lifetime in the comoving frame of the emission region can be of the order the dynamical time scale of the flare (e.g. in Gamma Ray Bursts). Moreover, their synchrotron losses are by a factor $(m_p/m_\star)^3 \sim 10^3$ stronger than for protons. Adiabatic cooling of muons has been considered for neutrino emission of Gamma-Ray Bursts [13], and synchrotron cooling of pion and muons has been discussed for extremely magnetized environments, e.g. neutron star magnetospheres [34]. Most of the literature about neutrino emission of AGN, however, neglects this effect. We will show here that this is not justified, and derive the critical Lorentz factors, $\hat{\gamma}_\star$, above which the energy loss of muons and pions plays a role. Obviously, we have to distinguish between neutrinos from the decay of pions and muons, because of their very different lifetimes. Energy losses of the muons are generally more relevant, which affects in particular the electron neutrinos, arising exclusively from muon decay. This is important for neutrino detection in UHE air shower experiments, where electron neutrino showers are easier to distinguish from the atmospheric background and are therefore proposed as providing most of the expected signal [35,11].

Pions and muons cool adiabatically prior to their decay if $\tau_\star \gamma_\star > 2B/\dot{B}$, which gives a critical Lorentz factor $\hat{\gamma}_\star = 2T\mathcal{D}\rho_T/\alpha\beta_{\text{ex}}\tau_\star$ for $B \propto R^{-\alpha}$, leading to

$$\tilde{\mathcal{E}}_{\nu,\text{ad}(\star)} = E_{\nu,\star}^{\text{RF}} \frac{2T\mathcal{D}^2\rho_T}{\alpha\beta_{\text{ex}}\tau_\star} . \quad (19)$$

Analogously, pions and muons can undergo efficient synchrotron cooling if $\gamma_\star^{\text{dc}}\tau_\star \leq t_{\star,\text{syn}}$. The critical Lorentz factor is thus found from $\gamma_b t_{\text{b,syn}}(m_\star/m_p)^3 = \hat{\gamma}_\star^2 \tau_\star$, yielding

$$\tilde{\mathcal{E}}_{\nu,\text{syn}(\star)} = \frac{3}{2} \frac{\omega_\star}{\omega_{B,\star}} E_{\nu,\star}^{\text{RF}} \mathcal{D} \quad \text{with} \quad \omega_\star = \sqrt{\frac{c}{\tau_\star r_\star}}, \quad (20)$$

where $r_\star = e^2/m_\star c^2$ is the classical radius of the particle, and $\omega_{B,\star} = eB/m_\star c$ its cyclotron frequency. The characteristic frequency, ω_\star , for synchrotron losses of pions and muon is found as $\omega_\pi = 3.3 \times 10^{16} \text{ s}^{-1}$ and $\omega_\mu = 3.2 \times 10^{15} \text{ s}^{-1}$, respectively. Pions and muons may also suffer inverse Compton (IC) losses from interactions with background photons. The corresponding cooling time is related to the synchrotron cooling time by the well known relation

$$t_{\star,\text{IC}} = t_{\star,\text{syn}} \frac{u_{\text{ph}}}{u_B} \approx t_{\star,\text{syn}} \frac{2\mathcal{L}_b G_a}{B^2 R_\parallel^2 c x_L} , \quad (21)$$

where G_a is a bolometric correction factor depending on the photon spectral index a ; for $a = 2$ we have $G_a \approx \ln(\hat{\epsilon}/\epsilon_b)$. For high pion and muon energies Eq. (21) might be modified by Klein-Nishina corrections, leading to a suppression of IC cooling.

Unlike the proton case, IC cooling is the most relevant process for photo-interactions of pions and muons. Their IC cooling time is related to the proton IC cooling time as $t_{\star,\text{IC}} = (m_\star/m_p)^3 t_{p,\text{IC}}$, while the Bethe-Heitler cooling time only scales with $t_{\star,\text{BH}} = (m_\star/m_p) t_{p,\text{BH}}$. For $a = 2$, one can show that $t_{\star,\text{BH}} \sim 5 t_{\star,\text{IC}}$, if Klein-Nishina corrections are disregarded. For the pion, there are additional channels due to meson resonance excitation; the lowest energy process is $\pi^\pm \gamma \rightarrow \rho^\pm \rightarrow \pi^\pm \pi^0$, which has a theoretical peak cross section of $\sim 50 \text{ pbarn}$ (determined from the $\rho^\pm \rightarrow \pi^\pm \gamma$ decay branching ratio by use of the Breit-Wigner formula [36]), at a photon energy of $\epsilon_{\pi \rightarrow \rho} \sim 2 \text{ GeV}$ in the pion rest frame. Compared to the pion production off the proton via the Δ -resonance, where the characteristic photon energy is $\epsilon_{p \rightarrow \Delta} \sim 300 \text{ MeV}$, this interaction is suppressed by a factor $\sim \frac{1}{6}(\epsilon_{p \rightarrow \Delta}/\epsilon_{\pi \rightarrow \rho})^a$; for $a \approx 2$, and neglecting the finite lifetime of the pion, secondary photon scattering has a probability of $< 0.3\%$, and can thus be neglected. However, the process may be relevant in inverted photon spectra, e.g. for pion production in the Rayleigh-Jeans part of the thermal background.

2. Spectral modification at the critical energies

The “maximum” neutrino energies derived in Sect. III B arise from the balance of energy gain and loss processes. The stochastic nature of these processes allows the particles to exceed such “limits” with some, usually exponentially decreasing probability. This has been shown for Fermi accelerated particles subject to synchrotron losses [37,38], which show a largely unmodified extension of the power law spectrum up to the cutoff energy (defined by balance of gains and losses), followed by an exponential-like cutoff; depending on the detailed parameters, a pile-up may occur at the cutoff energy. Although the stochastic behavior of photohadronic losses is quite different from synchrotron losses, we may expect a similar result in this case, and also for adiabatic losses. In general, we can assume that if the neutrino energy is limited by the maximum proton energy, the spectrum will continue as an approximate power law up to $\hat{\mathcal{E}}_\nu$, and drop off rapidly for $\mathcal{E}_\nu > \hat{\mathcal{E}}_\nu$.

The situation is different for the decay of unstable particles, where the particle can decay within a time Δt after its production with a probability $P_{\text{dc}} = 1 - \exp(-\Delta t/t_{\text{dc}})$. Far above the critical Lorentz factor, $\gamma_\star^{\text{dc}} \gg \hat{\gamma}_\star$, the decay probability within a cooling time scale $t_{\text{cool}} \ll t_{\text{dc}}$ in the fluid frame can then be approximated as $P_{\text{dc}}(t_{\text{cool}}) \approx t_{\text{cool}}/t_{\text{dc}} = t_{\text{cool}}/\gamma_\star \tau_\star$. The critical Lorentz factor is defined by the condition that $t_{\text{cool}}(\hat{\gamma}_\star) = \hat{\gamma}_\star \tau_\star$, which allows us to write $t_{\text{cool}} = t_{\text{dc}}(\gamma_\star/\hat{\gamma}_\star)^w$. For adiabatic

cooling, $t_{\text{cool}} = \text{const}(\gamma_*)$ means $w = 1$, while for synchrotron cooling we have $w = 2$. Cooling by secondary photon scattering — if relevant — would correspond to $w = a$.

For pions or muons produced with $\gamma_*^{\text{pr}} \lesssim \hat{\gamma}_*$, neutrinos are produced with an energy $\mathcal{E}_\nu \approx E_{\nu,*}^{\text{RF}} \gamma_* \mathcal{D}$ in the observers frame, and their power spectrum is $\bar{\mathcal{L}}_\nu \propto \mathcal{E}_\nu^q$, as discussed in Sect. II B. For $\gamma_*^{\text{pr}} \gg \hat{\gamma}_*$, the power spectrum is modified by the probability to decay within a cooling time $t_{\text{cool}}(\gamma_*^{\text{pr}})$, i.e.

$$\bar{\mathcal{L}}_\nu \propto \mathcal{E}_\nu^q P_{\text{dc}}(t_{\text{cool}}) \Big|_{\gamma_* = \mathcal{E}_\nu / \mathcal{D} E_{\nu,*}^{\text{RF}}} \propto \mathcal{E}_\nu^{q-w} \quad \text{for } \mathcal{E}_\nu \gg E_{\nu,*}^{\text{RF}} \hat{\gamma}_* \mathcal{D} . \quad (22)$$

Therefore, the critical Lorentz factor marks a spectral break of magnitude $\Delta q = -w$, rather than an exponential cutoff. Clearly, this simplified analytical estimate does not treat exactly the energy evolution of the pions and muons, thus neglects particle number conservation. Considering this would lead to a pile-up of decaying pions and muons around their respective critical Lorentz factor, before the spectrum turns over into a \mathcal{E}_ν^{q-w} behavior. The strength of the pile-up is correlated to the magnitude of the spectral break, and is therefore expected to be stronger for synchrotron cooling breaks than for adiabatic cooling breaks.

Shall we now consider the critical energies of pion and muon cooling as break energies or as cutoff energies? Strictly speaking, they are break energies, because they just change the power law index of the spectrum, rather than turning over into an exponential behavior. The break due to adiabatic cooling of pions and muons is comparable to the spectral breaks occurring at transition points between different proton cooling processes, as given by Eq. (9a). The $\Delta q = -2$ break caused by synchrotron cooling, however, can be easily confused with an exponential steepening: it causes a drop of events of one order of magnitude over half a decade in energy, similar to the exponential function around its critical energy. We will therefore consider $\tilde{\mathcal{E}}_{\nu,\text{syn}(*)}$ as a cutoff energy of the neutrino spectrum hereafter, and compare it with the cutoff energies due to proton cooling as derived in Sect. III B, while $\tilde{\mathcal{E}}_{\nu,\text{ad}(*)}$ is treated as a break energy.

D. Model-independent discussion of spectral shapes, maximum energies and fluxes

1. The parameter space

The free parameters describing a transient fall into two classes: (i) observable parameters, i.e. the characteristic time scale, \mathcal{T} , and the isotropized luminosity, \mathcal{L} , and (ii) theoretical parameters, like B , \mathcal{D} , θ_F , etc. We consider the former as given for any specific transient (disregarding possible problems in their determination, c.f. Sect. III A 2); the latter can usually be constrained through general physical considerations or additional observations within a certain range. However, inspection of Eqs. (15) shows that the maximum energies depend strongly on these parameters, in particular on the magnetic field B and the Doppler factor \mathcal{D} . In contrast, the hydrodynamic parameters of the flow, i.e. α , β_{ex} and β_{sh} are of order unity, and can generally be recast into some reasonable assumption for ρ_L . A special role is played by θ_F , which describes the speed of the acceleration process: as shown in Appendix C, first and second order Fermi acceleration is limited to $\theta_F > 1$; but we could easily consider any faster acceleration process in our analysis by inserting the appropriate θ_F . We therefore shall use θ_F as a fixed parameter, with the canonical assumption that $\theta_F \approx 1$, while B and \mathcal{D} span the two-dimensional parameter space describing a transient.

From Eqs. (15) we can immediately derive a qualitative division of the parameter space:

1. For each given \mathcal{D} , synchrotron losses of protons dominate over both photohadronic or adiabatic (Larmor) limits for magnetic fields larger than some value $\tilde{B}_{\text{syn}(p)}(\mathcal{D})$. Analogously, there is a magnetic field $\tilde{B}_{\text{syn}(*)}(\mathcal{D})$ above which muon or pion synchrotron losses dominate over all other proton loss processes; the relation of $\tilde{B}_{\text{syn}(p)}(\mathcal{D})$ and $\tilde{B}_{\text{syn}(*)}(\mathcal{D})$ depends on the other parameters.
2. For each given B photohadronic interactions of protons dominate over both synchrotron and adiabatic (Larmor) limits for Doppler factors smaller than some value $\hat{\mathcal{D}}_{p\gamma}(B)$. Similarly, there is a limit $\hat{\mathcal{D}}_{p\gamma,*}$ below which photohadronic interactions also dominate over pion or muon synchrotron cooling.
3. For each given \mathcal{D} , there is a limiting magnetic field $\hat{B}_{\text{ad}(p)}(\mathcal{D})$ below which adiabatic or Larmor limits dominate over synchrotron or photohadronic cooling of protons, and another value $\hat{B}_{\text{ad}(p),*}$ below which it dominates over either muon or pion synchrotron cooling.

It is much more difficult to determine under which conditions adiabatic cooling of pions and muons dominate; we will see in Sect. IV B that, if at all, this can happen only in a very limited region of the parameter space. For a more illustrative discussion of the parameter space constraints specific to AGN jets and Gamma Ray Bursts see Sect. IV A 2 and Sect. IV B 2, and the figures shown there.

To get a quantitative idea about the above parameter space division, we derive the condition under which the delimiting energies $\hat{\mathcal{E}}_{\nu,\text{syn}(p)}$, $\hat{\mathcal{E}}_{\nu,p\gamma}$ and $\hat{\mathcal{E}}_{\nu,\text{L}(p)}$ are all equal. This is equivalent to the condition $t_{\text{ad}} = t_{p,\text{syn}} = t_{p\gamma} = t_{\text{acc}}$, representing

three equations which can be solved for the three variables B , \mathcal{D} and γ_p . The corresponding solutions for the magnetic field and Doppler factor are called B^* and \mathcal{D}^* , and the corresponding solution for the maximum proton Lorentz, $\hat{\gamma}_p^*$, factor gives the maximum neutrino energy at this point, $\hat{\mathcal{E}}_\nu^* = \frac{1}{4}m_\pi c^2 \mathcal{D}^* \hat{\gamma}_p^*$. For the case $\hat{\gamma}_p \leq \gamma_b$, we find

$$\mathcal{D}^* = \left[\left(\frac{\Xi_\tau}{\alpha \beta_{\text{ex}} \theta_F^2} \right)^{a-1} \left(\frac{\Upsilon_1}{\alpha \beta_{\text{ex}}} \right)^3 \right]^{\frac{1}{2a+10}} \quad (23a)$$

$$B^* = \frac{m_p^2 c^4}{e^3} \frac{9 \theta_F \alpha \beta_{\text{ex}}}{8 \pi \Xi_\tau \hat{\gamma}_b^2} \left[\frac{\Xi_\tau^2}{\Upsilon_1 \alpha \beta_{\text{ex}} \theta_F^4} \right]^{\frac{1}{a+5}} \quad (23b)$$

$$\hat{\mathcal{E}}_\nu^* = \frac{m_\pi c^2 \hat{\gamma}_b}{4} \left[\left(\frac{\Xi_\tau^2}{\alpha \beta_{\text{ex}} \theta_F^4} \right)^{a+1} \frac{\Upsilon_1^4}{(\alpha \beta_{\text{ex}})^5} \right]^{\frac{1}{2a+10}} \quad (23c)$$

where we introduced the dimensionless quantity

$$\Xi_\tau \equiv \left(\frac{3}{4\pi} \right)^2 \frac{c \mathcal{T} \rho_T}{r_p \hat{\gamma}_b^3}$$

The relations for the case $\hat{\gamma}_p \gg \gamma_b$ are obtained from Eqs. (23) by setting $a = 1$ and use the proper value of Υ_1 in Eq. (18). Eqs. (23) define a unique reference point in the parameter space of magnetic field and Doppler factor, which allows the discussion of the relation of cooling processes of the proton independent of any other physical properties of the transient. For notational simplicity, we refer to it as the *star-point* hereafter.

For some applications it is useful to normalize the magnetic field energy density by the comoving photon energy density. This is because the magnetic field and relativistic particles are often found to be nearly in equipartition (e.g. in the interstellar medium), and usually can assume that the radiative efficiency of electrons is 1, i.e. $u_{\text{ph}} = u_e$. We introduce the parameter

$$\xi_{B\gamma} \equiv \frac{u_B}{u_{\text{ph}}} = \frac{c^3 \rho_T^2 \mathcal{T}^2 B^2 \mathcal{D}^6}{2 b_L \mathcal{L}_b} \quad (24)$$

where the bolometric correction factor b_L correlates the total luminosity of the source between ϵ_b and the cutoff at $\hat{\epsilon}$ to its specific luminosity at ϵ_b ; for $a \not\approx 2$ this is $b_L \approx (\hat{\epsilon}/\epsilon_b)^{2-a}/|2-a|$, and $b_L \approx \ln(\hat{\epsilon}/\epsilon_b)$ for $a \approx 2$. In hadronic models, equipartition does not usually mean $\xi_{B\gamma} \sim 1$, because the protons contribute to the energy density of relativistic particles, and we expect $u_p + u_e \sim u_B$. In this case, $\xi_{B\gamma}$ can be used as a measure for the ratio of proton and electron energy densities, and $\xi_{B\gamma} \gg 1$ is a viable possibility, if the acceleration process works more efficiently for protons. The star-point value of $\xi_{B\gamma}$ is then found as

$$\xi_{B\gamma}^* = \left[18 \Upsilon_1^7 \Upsilon_2^5 \Xi_\tau (\pi \theta_F)^8 (\alpha \beta_{\text{ex}})^2 \left(\frac{27 \Upsilon_1^3 \Upsilon_2}{32 \pi \alpha \beta_{\text{ex}} \theta_F^4} \right)^a \right]^{\frac{1}{5+a}} , \quad (25)$$

where $\Upsilon_2 \equiv m_p c^3 \hat{\gamma}_b^2 / r_p b_L \mathcal{L}_b$.

2. General upper limits on the neutrino energy

For any given Doppler factor, the highest neutrino energy can be achieved for $B = \check{B}_{\text{syn(p)}}(\mathcal{D})$; this is because $\hat{\mathcal{E}}_{\nu, \text{L(p)}}$ and $\hat{\mathcal{E}}_{\nu, p\gamma}$ increases with increasing B , while $\hat{\mathcal{E}}_{\nu, \text{syn(p)}}$ decreases. The equations determining $\check{B}_{\text{syn(p)}}$ are $\hat{\mathcal{E}}_{\nu, \text{L(p)}} = \hat{\mathcal{E}}_{\nu, \text{syn(p)}}$ for $\mathcal{D} < \mathcal{D}^*$, and is $\hat{\mathcal{E}}_{\nu, p\gamma} = \hat{\mathcal{E}}_{\nu, \text{syn(p)}}$ for $\mathcal{D} \geq \mathcal{D}^*$, leading to

$$\check{B}_{\text{syn(p)}} = B^* (\mathcal{D}/\mathcal{D}^*)^{-k} \quad \text{for } \mathcal{D} < \mathcal{D}^* \quad (26a)$$

$$\check{B}_{\text{syn(p)}} = B^* (\mathcal{D}/\mathcal{D}^*)^{-2/3} \quad \text{for } \mathcal{D} \geq \mathcal{D}^* , \quad (26b)$$

with $k = 2+4/(a+2)$ in the case $\hat{\gamma}_p \lesssim \gamma_b$, and $k = \frac{10}{3}$ for $\hat{\gamma}_p \gg \gamma_b$. If we use $\xi_{B\gamma}$ as a coordinate of the parameter space instead of B , and the maximum neutrino energy is reached on the line $\xi_{B\gamma} = \xi_{B\gamma}^* (D/\mathcal{D}^*)^{14/3}$ for $\mathcal{D} > \mathcal{D}^*$, and $\xi_{B\gamma} = \xi_{B\gamma}^* (D/\mathcal{D}^*)^{6-2k}$ otherwise. This provides an upper limit for the maximum neutrino energy as a function of \mathcal{D}

$$\hat{\mathcal{E}}_\nu \leq \hat{\mathcal{E}}_{\nu,p}(\mathcal{D}) = \hat{\mathcal{E}}_\nu^*(\mathcal{D}/\mathcal{D}^*)^{1+k/2} \quad \text{for } \mathcal{D} < \mathcal{D}^* \quad (27a)$$

$$\hat{\mathcal{E}}_\nu \leq \hat{\mathcal{E}}_{\nu,p}(\mathcal{D}) = \hat{\mathcal{E}}_\nu^*(\mathcal{D}/\mathcal{D}^*)^{4/3} \quad \text{for } \mathcal{D} \geq \mathcal{D}^* \quad . \quad (27b)$$

Stronger constraints on $\hat{\mathcal{E}}_\nu$ may exist from secondary particle cooling. We will only consider synchrotron cooling, because the impact of adiabatic cooling of decaying particles on the neutrino spectral shape is relatively weak, as argued in Sect. III C 2; moreover, it is often dominated by the other cooling processes, as we will see in Sect. IV. From the conditions $\tilde{\mathcal{E}}_{\nu,\text{syn}(\star)} = \hat{\mathcal{E}}_{\nu,p\gamma}$ for $\mathcal{D} \lesssim \mathcal{D}^*$, and $\tilde{\mathcal{E}}_{\nu,\text{syn}(\star)} = \hat{\mathcal{E}}_{\nu,\text{L(p)}}$ otherwise, we find the solutions for the magnetic field

$$\check{B}_{\text{syn}(\star)}(\mathcal{D}) \approx \check{B}_{\text{syn}(\star)}^*(\mathcal{D}/\mathcal{D}^*)^{-k_*} \quad \text{for } \mathcal{D} \lesssim \mathcal{D}^* \quad (28a)$$

$$\check{B}_{\text{syn}(\star)}(\mathcal{D}) = \check{B}_{\text{syn}(\star)}^*(\mathcal{D}/\mathcal{D}^*)^{-1/2} \quad \text{for } \mathcal{D} \gtrsim \mathcal{D}^* , \quad (28b)$$

where $k_* = 1 + 3/(a + 1)$, and $\check{B}_{\text{syn}(\star)}^* = \sqrt{\alpha\beta_{\text{ex}}\theta_F B_T B_* / 2\mathcal{D}^*}$ with $B_T \equiv \pi m_p c / e \rho_T T$ and $B_* \equiv 3m_* \omega_* c / e$. Using $\xi_{B\gamma}$ as a variable, we obtain $\xi_{B\gamma} \approx \check{\xi}_{B\gamma,\text{syn}(\star)}^* (\mathcal{D}/\mathcal{D}^*)^{6-2k_*}$ and $\xi_{B\gamma} = \check{\xi}_{B\gamma,\text{syn}(\star)}^* (\mathcal{D}/\mathcal{D}^*)^5$, respectively, with

$$\check{\xi}_{B\gamma,\text{syn}(\star)}^* = \frac{\alpha\beta_{\text{ex}}\theta_F c^3 \rho_T^2 T^2 B_T B_* \mathcal{D}^{*5}}{2b_L \mathcal{L}_b} \quad (29)$$

The transition from photohadronic to adiabatic dominance at $B = \check{B}_{\text{syn}(\star)}(\mathcal{D})$ is exactly at $\mathcal{D} = \mathcal{D}^*$ in the case $\hat{\gamma}_p \gg \gamma_b$. For $\hat{\gamma}_p \leq \gamma_b$ the exact transition value could be easily found by setting Eq. (28a) and Eq. (28b) equal and solving for \mathcal{D} , but the approximate division at \mathcal{D}^* will usually be adequate in practice. We also have to compare $\check{B}_{\text{syn}(\star)}(\mathcal{D})$ with $\check{B}_{\text{syn}(p)}(\mathcal{D})$; only for $\check{B}_{\text{syn}(\star)}(\mathcal{D}) < \check{B}_{\text{syn}(p)}(\mathcal{D})$ does secondary particle cooling determine the maximum energy. In this case, the upper limits to the neutrino energy are

$$\hat{\mathcal{E}}_\nu \leq \hat{\mathcal{E}}_{\nu,\star}(\mathcal{D}) = \hat{\mathcal{E}}_\nu^*(\mathcal{D}/\mathcal{D}^*)^{k_*+1} \quad \text{for } \mathcal{D} \lesssim \mathcal{D}^* \quad (30a)$$

$$\hat{\mathcal{E}}_\nu \leq \hat{\mathcal{E}}_{\nu,\star}(\mathcal{D}) = \hat{\mathcal{E}}_\nu^*(\mathcal{D}/\mathcal{D}^*)^{3/2} \quad \text{for } \mathcal{D} \gtrsim \mathcal{D}^* \quad (30b)$$

with

$$\hat{\mathcal{E}}_{\nu,\star}(\mathcal{D}^*) = E_{\nu,\star}^{\text{RF}} \mathcal{D}^{*3/2} \left[\frac{3}{2\pi} \frac{\rho_T T m_* \omega_*}{\alpha \beta_{\text{ex}} \theta_F m_p} \right]^{\frac{1}{2}}$$

A more illustrative discussion of the relation between $\check{B}_{\text{syn}(\star)}(\mathcal{D})$ and $\check{B}_{\text{syn}(p)}(\mathcal{D})$ in the different regions of the parameter space is given in Sect. IV.

3. Efficiency considerations and neutrino flux limits

The relevant question whether neutrinos above a certain energy from a specific class of sources can be observed or not, is usually not only whether this neutrino energy can be attained, but also which total neutrino luminosity is associated to this energy. This leads us to a more detailed discussion how the neutrino efficiency, defined in Eq. (31), behaves in the different regions of the parameter space, associated with different dominating cooling processes.

If we assume that $B < \check{B}_{\text{syn}(\star)}$, i.e. we are in the part of the parameter space where secondary particle cooling plays no role, then the neutrino efficiency can be written as $\zeta_\nu = \frac{1}{2} \bar{t}_p / t_{p,\pi}$, where the cooling time ratio is given by Eq. (7). If we are “deep” inside the dominance region of a specific process, we can moreover apply the maximum approximation in Eq. (7) and write $\zeta_\nu = \frac{1}{2} f_{\text{max}}^{-1}$. If we consider the efficiency at the maximum proton energy, $m_p c^2 \hat{\gamma}_p$, the description is also simple exactly at the border regions, where two or all cooling times are equal: e.g., at the border between adiabatic and synchrotron cooling (but far away from photohadronic dominance), we have $\hat{\zeta}_\nu = \frac{1}{4} f_{\text{ad}}^{-1}$. In the star-point, i.e. for $\mathcal{D} = \mathcal{D}^*$, $B = B^*$, and $\gamma_p = \hat{\gamma}_p^*$, we can easily derive $\zeta_\nu^* = (6f_{p\gamma}^*)^{-1}$, and we note that, unless $a > 2$ and Bethe-Heitler cooling plays a role, $f_{p\gamma}^* \approx 3$ can usually be assumed, leading to $\zeta_\nu^* \approx \frac{1}{18}$.

Using the scaling properties of the cooling times, this enables us to find simple expressions for the efficiencies in that regions of the parameter space, where one process clearly dominates:

- If photohadronic cooling dominates, we have

$$\zeta_\nu(\hat{\gamma}_p) \approx \hat{\zeta}_{\nu,p\gamma} \equiv \frac{1}{2} f_{p\gamma}^{-1} \quad \text{with} \quad f_{p\gamma} \approx 1 + \exp(5a - 10), \quad (31a)$$

which leads to $\hat{\zeta}_{\nu,\text{ad}} \approx \frac{1}{2}$ if $a \leq 2$, i.e. Bethe-Heitler losses can be neglected. In general, the total hadronic radiative efficiency in this region is ≈ 1 , which approximately equal parts (for $a \leq 2$) radiated in neutrino and electromagnetic channels. Cosmic ray ejection is generally suppressed by neutron reabsorption, and direct proton ejection can usually assumed to be marginal, except for special geometries and, maybe, at the highest energies.

- If synchrotron cooling dominates, we have

$$\zeta_\nu(\hat{\gamma}_p) \approx \hat{\zeta}_{\nu,\text{syn}} \equiv 3\zeta_\nu^* \left(\frac{B}{B^*}\right)^{-2} \left(\frac{\mathcal{D}}{\mathcal{D}^*}\right)^{-(4+a)} \left(\frac{\hat{\gamma}_p}{\hat{\gamma}_p^*}\right)^{a-2} \quad (31b)$$

Like in the case of photohadronic dominance, the total hadronic radiative efficiency is close to 1, but the predominant part of the energy is emitted in electromagnetic radiation.

- If adiabatic cooling dominates, we have

$$\zeta_\nu(\hat{\gamma}_p) \approx \hat{\zeta}_{\nu,\text{ad}} \equiv 3\zeta_\nu^* \left(\frac{\mathcal{D}}{\mathcal{D}^*}\right)^{-(3+a)} \left(\frac{\hat{\gamma}_p}{\hat{\gamma}_p^*}\right)^{a-1} \quad (31c)$$

Here, most of the energy is not radiated, but reconverted into kinetic energy of expansion. Thus, the total hadronic radiative energy decreases in total, while the distribution of the radiated energy between cosmic rays, neutrinos and photons remains constant, and approximately $2 : 1 : 1$ for $a \leq 2$.

Note that, instead of the star-point, any point in or at the border of the respective dominance region could be used as a reference point in Eqs. (31). If secondary particle cooling plays a role, the situation is principally similar to the case of proton cooling: For synchrotron cooling, the total hadronic radiative efficiency remains constant, but more energy is channeled into energetic photons; for adiabatic cooling, additional energy is reconverted in bulk kinetic energy. We do not discuss the scaling properties for these cases; rather, we will use $\check{\mathcal{E}}_{\nu,\text{syn}(\star)}$ as limiting energy and discuss the efficiencies only for $\mathcal{E}_\nu < \check{\mathcal{E}}_{\nu,\text{syn}(\star)}$, and we will neglect the effect of adiabatic cooling of secondary particles altogether.

The neutrino efficiency alone does not allow to derive flux rates; we also have to make assumptions about the energy density of relativistic protons in the source. Here we can use the standard equipartition argument discussed above, and introduce a parameter $\bar{\xi}_{pB} \equiv \bar{u}_p/u_B \sim 1$, which allows us to express the time integrated proton injection energy density, \bar{u}_p by the parameter space variable $\xi_{B\gamma}$ defined in Eq. (24). The neutrino luminosity at the maximum energy can then be expressed in units of \mathcal{L}_b by

$$\hat{\psi}_\nu \equiv \left. \frac{\bar{\mathcal{L}}_\nu}{b_L \mathcal{L}_b T} \right|_{\mathcal{E}_\nu = \check{\mathcal{E}}_{\nu}(\mathcal{D})} = A_s^{-1} \bar{\xi}_{pB} \xi_{B\gamma} \zeta_\nu \Big|_{\gamma_p = \hat{\gamma}_p(\mathcal{D})} \quad (32)$$

where $\hat{\gamma}_p$ denotes the maximum proton Lorentz factor attainable for a given \mathcal{D} , for which secondary particle cooling can yet be neglected, and A_s is the normalization factor for the proton energy spectrum introduced in (8). If $\check{B}_{\text{syn}(\star)}(\mathcal{D}) > \check{B}_{\text{syn}(p)}(\mathcal{D})$, this implies $\xi_{B\gamma}$ and $\hat{\zeta}_{\nu,\text{ad}}(\mathcal{D})$ have to be taken at $B = \check{B}_{\text{syn}(p)}(\mathcal{D})$ and we obtain

$$\hat{\psi}_{\nu,p} = \frac{\bar{\xi}_{pB} \xi_{B\gamma}^*}{4A_s f_{p\gamma}^*} \left(\frac{\mathcal{D}}{\mathcal{D}^*}\right)^{\frac{2a-4}{a+2}} \quad \text{for} \quad \mathcal{D} < \mathcal{D}^* \quad (33a)$$

$$\hat{\psi}_{\nu,p} = \frac{\bar{\xi}_{pB} \xi_{B\gamma}^*}{4A_s f_{p\gamma}^*} \left(\frac{\mathcal{D}}{\mathcal{D}^*}\right)^{\frac{4-2a}{3}} \quad \text{for} \quad \mathcal{D} \geq \mathcal{D}^* \quad (33b)$$

If $\check{B}_{\text{syn}(\star)}(\mathcal{D}) < \check{B}_{\text{syn}(p)}(\mathcal{D})$, $\xi_{B\gamma} = \check{\xi}_{B\gamma,\text{syn}(\star)}(\mathcal{D})$ has to be used for the appropriate scaling, and we obtain

$$\hat{\psi}_{\nu,*} \approx \frac{\bar{\xi}_{pB} \check{\xi}_{B\gamma,\text{syn}(\star)}^*}{4A_s f_{p\gamma}^*} \left(\frac{\mathcal{D}}{\mathcal{D}^*} \right)^{\frac{4a-2}{a+1}} \quad \text{for } \mathcal{D} < \mathcal{D}^* \quad (34a)$$

$$\hat{\psi}_{\nu,*} \approx \frac{\bar{\xi}_{pB} \check{\xi}_{B\gamma,\text{syn}(\star)}^*}{4A_s f_{p\gamma}^*} \left(\frac{\mathcal{D}}{\mathcal{D}^*} \right)^{\frac{3-a}{2}} \quad \text{for } \mathcal{D} \geq \mathcal{D}^* \quad (34b)$$

We note that, if secondary particle cooling plays no role, $\hat{\psi}_\nu$ is independent of \mathcal{D} for $a = 2$, and has a maximum for $\mathcal{D} = \mathcal{D}^*$ for $a > 2$. In case of the dominance of secondary particle cooling, a maximum is only obtained for $a \geq 3$, while otherwise $\hat{\psi}_\nu$ continues to rise with \mathcal{D} . Therefore, for given \mathcal{L}_b , both the maximum neutrino energy and the power flux at this energy increases with \mathcal{D} in most cases, and a general upper limit cannot be stated.

However, we have to consider that this result is mainly due to the extremely large values of $\xi_{B\gamma}$ required for large Doppler factors to reach the respective energy limit, $\hat{\mathcal{E}}_\nu(\mathcal{D})$. This, of course, increases also the total energy required to be dissipated into relativistic particles and magnetic fields by the transient, and may be compared to the total energy budget assumed in specific source models. Denoting the total dissipated energy of the transient, which can usually be constrained by fundamental principles, with \bar{E}_T , we can write

$$\xi_{B\gamma,\text{max}} = \frac{2\tilde{\xi}_{B\gamma,\text{max}}}{(1 + \tilde{\xi}_{pB})\Omega} \quad \text{with} \quad \tilde{\xi}_{B\gamma,\text{max}} = \frac{2\pi\bar{E}_T}{b_L \mathcal{L}_b} \quad (35)$$

if Ω is the total angle over which the energy is emitted; the case of a beamed source, i.e. when the energy is emitted in a thin jet, corresponds to $\Omega \approx \mathcal{D}^{-2}$. This allows to state an upper limit on the Doppler factor, $\hat{\mathcal{D}}$, for which $\hat{\mathcal{E}}_\nu = \hat{\mathcal{E}}_\nu$ and $\bar{\mathcal{L}}_\nu(\hat{\mathcal{E}}_\nu) = \hat{\psi}_\nu \bar{\mathcal{L}}$, with $\bar{\mathcal{L}} \equiv b_L \mathcal{L}_b \mathcal{T}$, can be attained; we confine the discussion to the case $\xi_{B\gamma,\text{max}} > \check{\xi}_{B\gamma,\text{syn}(\star)}^*$, which means $\hat{\mathcal{D}} > \mathcal{D}^*$, assuming $\check{B}_{\text{syn}(\star)} < \check{B}_{\text{syn}(p)}$ in the relevant range of Doppler factors. For the interesting case $\tilde{\xi}_{pB} = 1$ we then obtain from Eq. (30b)

$$\hat{\mathcal{E}}_\nu \leq E_{\nu,*}^{\text{RF}} \mathcal{D}^{*3/2} \left[\frac{\tilde{\xi}_{B\gamma,\text{max}}}{\check{\xi}_{B\gamma,\text{syn}(\star)}^* \Omega^*} \right]^{\lambda_1} \left[\frac{3}{2\pi} \frac{\rho_T \mathcal{T} m_\star \omega_\star}{\alpha \beta_{\text{ex}} \theta_F m_p} \right]^{\frac{1}{2}} . \quad (36)$$

with $\lambda_1 = \frac{3}{10}$ for $\Omega^* = \Omega = \text{const} > \hat{\mathcal{D}}^{-2}$, and $\lambda_1 = \frac{1}{2}$, $\Omega^* = \mathcal{D}^{-2}$ in the case of beamed emission. Eq. (36) is a true, *model-independent* upper limit for $\hat{\mathcal{E}}_\nu$: if we increase \mathcal{D} over $\hat{\mathcal{D}}$, keeping $\xi_{B\gamma} = \xi_{B\gamma,\text{max}}$, this means that $B \propto \mathcal{D}^{-3}$ for constant Ω , and $B \propto \mathcal{D}^{-2}$ for a collimated beam; since the maximum energy is determined by the adiabatic limit, Eq. (15a), this leads to $\hat{\mathcal{E}}_\nu \propto \mathcal{D}^{-1}$ and $\hat{\mathcal{E}}_\nu \propto \text{const}$, respectively. (If we consider lower Doppler factors, Eq. (30) limits the energy to values lower than in Eq. (36).) From Eq. (34b) we obtain

$$\hat{\psi}_\nu(\hat{\mathcal{D}}) = \frac{\check{\xi}_{B\gamma,\text{syn}(\star)}^*}{4f_{p\gamma}^*} \left[\frac{\tilde{\xi}_{B\gamma,\text{max}}}{\check{\xi}_{B\gamma,\text{syn}(\star)}^* \Omega^*} \right]^{\lambda_2} \quad (37)$$

with $\lambda_2 = (3-a)/10$ for $\Omega = \text{const}$ and $\lambda_2 = (3-a)/6$ in the beamed case, Ω^* assigned as above. Eq. (32) is not an upper limit, because higher values are generally allowed for lower Doppler factors; thus, one can increase the emitted neutrino power compared to the value in Eq. (37) on the expense of the maximum neutrino energy.

For other cases, such as $\hat{\mathcal{D}} < \mathcal{D}^*$ or $\check{B}_{\text{syn}(p)}(\hat{\mathcal{D}}) < \check{B}_{\text{syn}(\star)}(\hat{\mathcal{D}})$, the derivation of equivalent expressions is straightforward; some of these cases will be discussed in specific applications in the next section.

IV. NEUTRINO EMISSION FROM UNSTEADY ASTROPHYSICAL SOURCES

In this section, we apply the general theory developed in Sect. III to specific models of astrophysical transients, which are commonly discussed in the literature. Our aim is to explore the parameter space of these models more extensively than usually done in the literature, and to check the results for consistency with the limits set by secondary particle cooling, which is disregarded in most papers. To simplify the discussion, we ignore in the following the geometric parameters x_L and ρ_T introduced in the last section, and assume $x_L = \rho_T = 1$. However, since all times are normalized by the size of the emission region, and all luminosities by the photon energy density in the comoving frame, they can easily be re-introduced by replacing $\mathcal{T} \rightarrow \mathcal{T} \rho_T$ and $\mathcal{L} \rightarrow \mathcal{L}/x_L$ in all equations of this section.

A. Neutrinos from AGN jets

There are two classes of AGN models which predict neutrino emission, both involving normal e, p flows. One class involves particle acceleration at shocks in the accretion flow very close to the black hole, and produce neutrinos by both $p\gamma$ and pp interactions [5,39,7,9]. The other applies to radio loud AGN, which show extended radio jets, and locates the emission region at internal shocks in the relativistic jets at larger distances from the black hole [8,9]. The highest energy neutrinos would then be expected from *blazars*, which are AGN jets pointing in the direction of the observer, because the energy is boosted by the Doppler factor $\mathcal{D} \sim \Gamma_{\text{jet}} \gg 1$ [40]. We discuss this class of models, i.e. the *AGN jet models*, in the following; some interesting implications of our results on the other class, the *AGN core models*, are described in Appendix D.

1. The “proton blazar” scenario

Blazars are known to emit electromagnetic radiation from radio wavelengths up to the TeV-gamma ray regime. Their spectrum shows a typical “two-hump” structure, where characteristic photon energies depend on the source luminosity: In high luminosity blazars, such as 3C 279, the lower hump cuts off at optical wavelengths, while the high energy emission extends up to at least 10 GeV; in low luminosity sources, like in the nearby objects Mkn 421 and Mkn 501, the lower hump extends in flares up to 10–100 keV [41,42], and the high energy emission is observed up to $\gtrsim 10$ TeV [14,15]. While there is agreement that the low energy hump is due to synchrotron emission of energetic electrons, the origin of the high energy emission is unclear: It can be explained (a) by inverse-Compton emission of the same electron population producing the low energy synchrotron radiation (e.g. [18,43], and references therein), which could arise also if the jets are leptonic (consisting of e^\pm and magnetic fields, with few or no protons); or (b) by hadronically induced electromagnetic cascades, as described in Sect. II A. The latter mechanism is referred to as the “proton blazar” or hadronic scenario, and gives rise to considerable neutrino fluxes [16,8], while the leptonic models obviously do not. On the basis of gamma ray observations alone, the issue of the dominant radiation process in AGN jets is not settled yet (see [44,45], and references therein), even though the recent observations of photon energies above 5 TeV from Mkn 421 and Mkn 501 could be more naturally explained in the hadronic scenario [46]; the observation of correlated neutrinos could resolve this issue.

The typical bulk Lorentz factors Γ_{jet} of AGN jets can be estimated from the apparent superluminal motion of blobs in the jet; a recent investigation of 43 AGN indicates that $\Gamma_{\text{jet}} \lesssim 30$ [47], and the typical inclination angle of the blazar jets to the line of sight is inferred to be $\langle \Theta_{\text{view}} \rangle_{\text{bl}} \sim 5^\circ$, confirming the estimate $\mathcal{D} \sim \Gamma_{\text{jet}} \sim 10$ obtained from AGN unification models [48]; we may use $\mathcal{D} \lesssim 30$ as a “soft” upper limit on blazar Doppler factors. A lower limit on the Doppler factor of TeV blazars can be found from the observed emission of photons with $\epsilon \sim 1$ TeV, where the emission region must be optically thin with respect to $\gamma\gamma \rightarrow e^+e^-$ reactions of γ -rays on intrinsic soft photons, which leads to $\mathcal{D} \gtrsim 2\mathcal{L}_{x,45}^{1/5}\mathcal{T}_4^{-1/5}$. For crude estimates, we may use $\mathcal{D} \gtrsim 3$ as a lower limit for TeV blazars, since X-ray luminosities up to $\mathcal{L}_x \sim 10^{45}$ erg sec $^{-1}$ and variability time scales down to $\mathcal{T} \sim 10^3$ s are observed. A similar limit is obtained for the high luminosity blazar 3C 279, using EGRET observations and assuming the emission to be optically thin at 1 GeV [33].

In contrast to the bulk Lorentz factor, the magnetic field strength in blazars is more difficult to estimate, although hadronic models typically invoke $B \gtrsim 10$ G based on equipartition arguments [49]. A test of this claim is possible by observing the synchrotron-self absorption frequency of the *variable* emission of blazars; an analysis of the spectral shape and the multifrequency variability of blazars suggests that this turnover is at an observed frequency ~ 300 GHz [50]. Boosting into the comoving frame of the blob with $\mathcal{D} \lesssim 10$, this would be consistent with synchrotron-self absorption for $B \sim 10$ G and a relativistic electron energy density $u_e \ll B^2/8\pi$, which is expected in hadronic models [16]. Fields of this strength would also allow magnetic confinement of the jets, and would therefore help to explain the large scale jets observed in luminous radio galaxies, which extend from galactic scales (\gtrsim kpc) up to ~ 1 Mpc [51].

The emission from blazars is strongly variable, with activity periods taking turns with quiescent periods on a typical time scales of months [52]; this kind of long-term variability is observed at all frequencies, and appears to be largely correlated. Also within an activity period, the TeV emission from Mkn 421 and Mkn 501 shows clearly separated flares with doubling time scales from days down to less than one hour [15,53], i.e. $\mathcal{T} \sim 10^3\text{--}10^6$ s, with correlated variability of the synchrotron emission at X-ray energies [54]. This suggests an identification of these short-term flares with transient, causally disconnected acceleration regions of energetic particles, as e.g. expected in the scenario of internal shocks in the jets.

2. The parameter space for time-integrated neutrino spectra from blazar flares

We may assume that the relevant target photons for photohadronic pion production are the synchrotron photons in the low energy spectral hump produced by accelerated electrons, since the number density of photons in the high energy bump is too low and can be neglected. The target photon spectrum in the comoving frame of the relativistic flow can then be approximated by a

power law with a typical index $\langle a \rangle \approx 1.7$, if we use a power law interpolation between the sub-mm and X-ray wave bands [50], ignoring the observed break at optical frequencies; this is also justified by the observation that in flares the important optical-to-X-ray spectrum of low luminosity blazars seems to be flatter than the typical $\langle a_{\text{ox}} \rangle \approx 2$ seen in the quiescent state [54,42,55].³ In the following, we adopt $a = \frac{5}{3}$ and introduce the Doppler factor and magnetic field in canonical units, $\mathcal{D}_1 \equiv \mathcal{D}/10$, and $B_1 = B/10 \text{ G}$. For the break energy we use $\varepsilon_b \sim [10^{-4} \text{ eV}]$ [50], and $\hat{\varepsilon} \sim [1-10 \text{ keV}]$ from X-ray observations of flares in Mkn 421 and Mkn 501 [56,42]. The luminosity at the spectral break is not taken from observed fluxes at ε_b , because the emission at low energy is likely to be superposed by the emission from other jet regions not associated with the flare; rather, we use the observed, isotropized X-ray luminosity at $\varepsilon_x \approx 1 \text{ keV}$ of the flare and determine \mathcal{L}_b from scaling with the assumed power law photon spectrum, $\mathcal{L}_b = \mathcal{L}_{x,45} (\varepsilon_b/\varepsilon_x)^{1/3}$, where $\mathcal{L}_{x,45}$ is the X-ray luminosity in units of $10^{45} \text{ erg s}^{-1}$. Opacity requirements suggest that for low luminosity TeV blazars the external radiation does not dominate over the synchrotron component in the comoving frame of the flow [57]; if this would be the case, the thermal-like properties of the disk radiation would yield a neutrino spectra substantially different from our results.

For the characteristic Lorentz factor in the comoving frame we find $\gamma_b \sim [3 \times 10^{11}] \mathcal{D}$, which is of the order the maximum proton Lorentz factors observed in cosmic rays. We will show below that acceleration of protons in blazars cannot reach higher Lorentz factors, and confine ourselves to the case $\gamma < \gamma_b$. In order to ignore the upper limit in the photon spectrum, we have to require $\gamma_p \gtrsim 10^{6-7} \mathcal{D}_1$.

To estimate the relevant time scale for the transient emission, \mathcal{T} , we use the X-ray variability, where we have to consider *electron* cooling times of order $30 B_1^{-3/2} \mathcal{D}_1^{-1} \text{ s}$ in the observer frame, which for standard parameters are much shorter than the observed rise or decay times of the flare. This suggests that one can use Eq. (14), which explains the generally longer decay times by Lorentz boosting effects in transrelativistic internal shocks, rather than by slow cooling. We note that this is in contrast to the usual interpretation of \mathcal{T} as the doubling time of the flare, which assumes much longer cooling times expected in the weak magnetic fields required by purely leptonic emission models to explain $\mathcal{T}_\downarrow > \mathcal{T}_\uparrow$. The latter explanation may also apply to hadronic models, if second order Fermi acceleration plays a role, so that in principle $\mathcal{T} = \mathcal{T}_\downarrow - \mathcal{T}_\uparrow$ can only be considered as an upper limit. The typical time scales of blazar flares are then $\mathcal{T} \equiv [10^4 \text{ s}] \mathcal{T}_4$ with $0.1 \lesssim \mathcal{T}_4 \lesssim 10$, corresponding to a comoving linear size of the emission region $R_\parallel \sim [3 \times 10^{15} \text{ cm}] \mathcal{T}_4 \mathcal{D}_1$. The fact that we probably have to deal with transrelativistic shocks also suggests $\theta_F \approx 1$, which we assume in numerical estimates; in general, however, we keep θ_F as a free parameter.

In a free relativistic jet we have $t_{\text{ad}} \approx T_{\text{cr}}$, i.e. the emission region expands with the velocity of light; however, if magnetic confinement applies, we might expect $\beta_{\text{ex}} < 1$. Heuristically, we can express the value of β_{ex} by the opening angle of the jet, $\beta_{\text{ex}} \simeq \min(1, \Theta_{\text{jet}} \Gamma_{\text{jet}})$, and assume $\Theta_{\text{jet}} \lesssim \langle \Theta_{\text{view}} \rangle_{\text{bl}} \sim 0.1$, which means that $\Gamma_{\text{jet}} \sim 10$ corresponds to $\beta_{\text{ex}} \lesssim 1$. Hence, existing observations cannot decide whether magnetic confinement applies or not, but β_{ex} can be expected to be close to 1. On the other hand standard jet theory assumes that $B \propto R^{-1}$, i.e. $\alpha = 1$, but $\alpha = 2$ may apply if reconnection isotropizes the magnetic field as assumed in Gamma Ray Bursts [58]. Since β_{ex} and α always appear as a product in the equation, $\alpha \beta_{\text{ex}} \approx 1$ is a reasonable assumption, and will be used in the following. Note that $\alpha \beta_{\text{ex}} = \theta_F = 1$ corresponds to $\rho_L \approx \frac{1}{3}$, and is thus equivalent to the assumption that particles are accelerated up to their Larmor limit. Using these standard parameters, we find for the star-point of the parameter space

$$\mathcal{D}^* \approx 5.9 \times \mathcal{L}_{x,45}^{9/40} \mathcal{T}_4^{-7/40} \theta_F^{-1/10} \quad (38a)$$

$$B^* \approx 98 \text{ G} \times \mathcal{L}_{x,45}^{-3/20} \mathcal{T}_4^{-11/20} \theta_F^{2/5} \quad (38b)$$

$$\xi_{B\gamma}^* \approx 180 \times \mathcal{L}_{x,45}^{-3/40} \mathcal{T}_4^{-3/20} \theta_F^{1/5} \quad (38c)$$

$$\hat{\mathcal{E}}_\nu^* \approx 1.7 \times 10^{18} \text{ eV} \times \mathcal{L}_{x,45}^{3/10} \mathcal{T}_4^{1/10} \theta_F^{-4/5} \quad (38d)$$

Fig. 1 shows the different regions of dominant cooling at the maximum energies, and their associated spectral shapes, where we have scaled \mathcal{D}_1 and B_1 relative to the star-point values. Also shown are the positions of three observed AGN flares in the parameter space, for which we assumed the magnetic field to be in equipartition (a) with the radiation density, or (b) with the energy density of protons, $up = 100u_e$, corresponding to standard assumptions in hadronic blazar models, and a range of possible Doppler factors $0.3 \lesssim \mathcal{D}_1 \lesssim 3$. Comparison with the lines of dominance of muon and pion cooling corresponding to these flares shows that muon particle cooling can only play a role for short flares in scenario (b), if $\mathcal{D} \lesssim 10$; pion cooling is generally unimportant for usual hadronic AGN models. Hence, in most cases the neutrino energy is limited by Larmor radius constraints of the accelerated protons, consistent with earlier assumptions [16,10].

³We confine ourselves to the treatment of low luminosity TeV blazars. For high luminosity blazars, like 3C 279, in which the synchrotron component cuts off at optical frequencies, our power law approximation is not applicable, although a simple scaling of the physical conditions allows some qualitative statements on their neutrino emission properties as well.

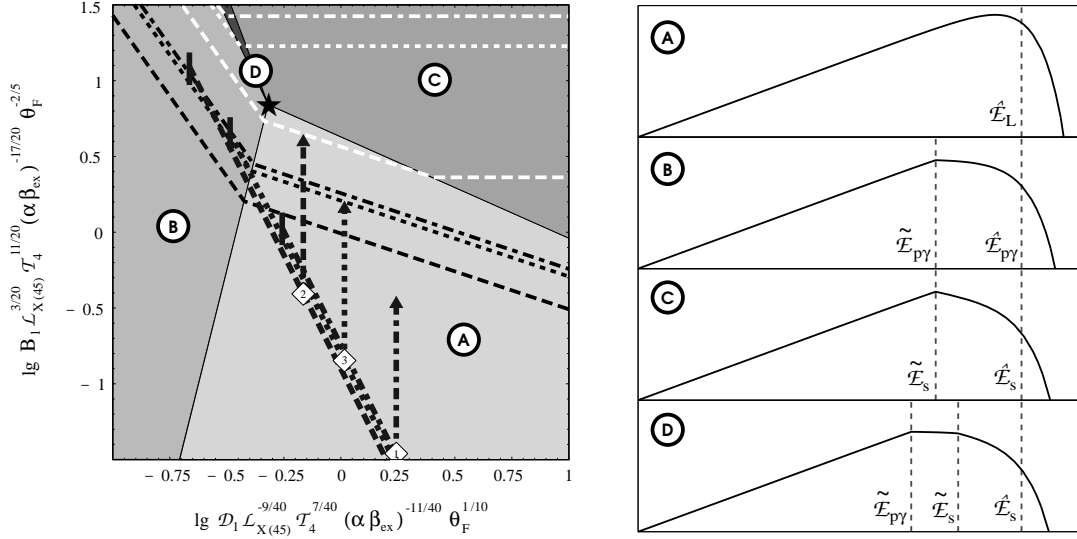


FIG. 1. Dominant cooling processes and neutrino spectral shapes for AGN jets — **Left:** Parameter space, with the “star-point”, denoting equal cooling time scales at the maximum energy, indicated. The shaded regions correspond to the dominant cooling process at the maximum proton energy: (A) Larmor limit or adiabatic cooling; (B) photohadronic cooling; (C) and (D) synchrotron cooling, where (D) marks the region where photohadronic cooling dominates for a part of the energy spectrum. Also shown are the positions of three observed AGN flares: $\langle 1 \rangle$ Mkn 421, April 26, 1995: $T_4 = 10$, $\mathcal{L}_{x,45} = 0.5$ [54]; $\langle 2 \rangle$ Mkn 421, May 7, 1996: $T_4 = 0.1$, $\mathcal{L}_{x,45} = 0.9$ [59]; $\langle 3 \rangle$ Mkn 501, April 16, 1997: $T_4 = 3$, $\mathcal{L}_{x,45} = 2.0$ [42]. Central positions assume $u_B = u_{ph}$, black triangles correspond to $u_B = 100u_{ph}$, diagonal errors indicate the range of possible Doppler factors (see text). Line styles of error bars correspond to the delimiting lines of muon cooling (black) and pion cooling (white); secondary particle cooling is relevant in the parameter space region above these lines. **Right:** Schematic representation of the shapes of neutrino spectra (time integrated power per logarithmic interval of energy), $\ln \bar{\mathcal{L}}_\nu(\mathcal{E}_\nu)$ vs. $\ln \mathcal{E}_\nu$, corresponding to regions (A)–(D).

3. Blazar neutrino maximum energies and fluxes

Keeping the magnetic field, the Doppler factor and the proton-to-electron energy ratio in blazars as free parameters, rather than adopting common assumptions, we can apply our discussion in Sect. III D to obtain general upper limits on neutrino energies and fluxes from this class of objects. We see from Fig. 1 that, for parameters typically observed in blazar flares, that $\check{B}_{\text{syn}(\mu)}(\mathcal{D}) < \check{B}_{\text{syn}(p)}(\mathcal{D})$, but $\check{B}_{\text{syn}(\pi)}(\mathcal{D}) \gtrsim \check{B}_{\text{syn}(p)}(\mathcal{D})$ for all Doppler factors in the discussed range. Therefore, $\mathcal{E}_\nu < \hat{\mathcal{E}}_{\nu,p}(\mathcal{D})$ applies to muon neutrinos from pion decay, and $\mathcal{E}_\nu < \hat{\mathcal{E}}_{\nu,\mu}$ to muon and electron neutrinos from muon decay.

To find out the relevant range for the Doppler factors, we start with energetical considerations. The usual limit applied to the power of AGN jets is the Eddington luminosity of the putative Black Hole in the AGN, i.e. $L_{\text{jet}} \lesssim [10^{47} \text{ erg/s}] M_{\text{BH},9}$, where $M_{\text{BH},9}$ is the mass of the Black Hole in units of $10^9 M_\odot$. Inserting in Eq. (35) assuming an energy dissipation efficiency of $\xi_{\text{sh}} \sim 0.2$ in the jet, as expected for transrelativistic internal shocks, we obtain $\xi_{B\gamma,\text{max}} \sim 42 M_{\text{BH},9} \mathcal{L}_{x,45}^{-1}$. Since we consider a beamed emitter, we have to set $\Omega = \mathcal{D}^{-2}$, and we find as the limiting Lorentz factor allowing $\hat{\mathcal{E}}_{\nu,\pi} = \hat{\mathcal{E}}_{\nu,\pi}$

$$\hat{\mathcal{D}}_\pi \approx 13 \times M_{\text{BH},9}^{3/8} T_4^{-1/4} \theta_F^{-1/4} \quad (39)$$

For the canonical range of assumed AGN Black Hole masses, $0.1 \lesssim M_{\text{BH},9} \lesssim 10$, we can therefore assume that $\hat{\mathcal{D}}_\pi > \mathcal{D}^*$, for which case we find

$$\hat{\mathcal{E}}_{\nu,\pi}(\mathcal{D}_1) \approx 3.6 \times 10^{18} \text{ eV} \times D_1^{4/3} T_4^{1/3} \theta_F^{-2/3} < [8 \times 10^{18} \text{ eV}] M_{\text{BH},9}^{1/2} \theta_F^{-1} \quad (40a)$$

$$\hat{\psi}_{\nu,\pi}(\mathcal{D}_1) \approx 1.25 \times D_1^{2/9} T_4^{-1/9} \theta_F^{2/9} < 1.3 M_{\text{BH},9}^{1/12} T_4^{-1/6} \theta_F^{1/6}, \quad (40b)$$

where we assumed $\xi_{pB} = 1$ and $A_s = 20$. Adopting these parameters, neutrinos from muon decay are limited by muon synchrotron cooling to an energy $\hat{\mathcal{E}}_{\nu,\mu} \lesssim [5 \times 10^{17} \text{ eV}] M_{\text{BH},9}^{5/8} T_4^{1/4} \theta_F^{-3/4}$. On the other hand, we can find the conditions under which neutrinos from muon decay, in particular electron neutrinos, can reach their highest energies and fluxes. We determine $\xi_{B\gamma,\text{syn}(\pi)}^* \approx 19 \mathcal{L}_{x,45}^{1/8} T_4^{1/8} \theta_F^{1/2}$, leading to

$$\hat{\mathcal{D}}_\mu \approx 30 M_{\text{BH},9}^{1/3} T_4^{-1/3} \theta_F^{-1/3} \quad (41)$$

Again we can confine the discussion to the case $\hat{\mathcal{D}}_\mu > \mathcal{D}^*$, which gives

$$\hat{\mathcal{E}}_{\nu,\mu}(\mathcal{D}_1) \approx 1.4 \times 10^{18} \text{ eV} \times D_1^{3/2} \mathcal{T}_4^{1/2} \theta_F^{-1/2} < [8 \times 10^{18} \text{ eV}] M_{\text{BH},9}^{1/2} \theta_F^{-1} \quad (42\text{a})$$

$$\hat{\psi}_{\nu,\mu}(\mathcal{D}_1) \approx 0.1 \times D_1^{2/3} \theta_F^{3/5} < 0.2 M_{\text{BH},9}^{2/9} \theta_F^{1/3}. \quad (42\text{b})$$

The result that the upper energy limits for neutrinos from pion and muon decay, in their respective optimization, are equal is not accidental; as discussed in Sect. III D 2, the maximum energy of pion neutrinos for Doppler factors $\mathcal{D} > \hat{\mathcal{D}}_\pi$ remains unchanged at $\hat{\mathcal{E}}_{\nu,\pi}$; since the optimization considers the maximum magnetic field for which the neutrino energy is still limited by adiabatic cooling, i.e. $\gamma_\mu^{\text{dc}} \approx \gamma_\pi^{\text{dc}} \approx \hat{\gamma}_p$, the upper limit given in Eq. (42a) has to apply to neutrinos from pion and muon decay as well, and since $\hat{\mathcal{D}}_\mu > \hat{\mathcal{D}}_\pi$ it has to be the same as in Eq. (40a). For the assumed range of AGN Black Hole masses and $\theta_F \gtrsim 1$, we therefore obtain a *strict* upper limit of about 2×10^{19} eV for neutrinos from AGN flares, which is independent of the flare time scale and any model assumptions. The inverse linear dependence on θ_F , however, shows that this energy limit would strongly increase if we assume acceleration on time scales much shorter than the particles Larmor motion.

The limit on the emitted neutrino power, however, strongly decreases with increasing \mathcal{D} ; if the TeV emission from blazars ought to be explained by hadronic emission, the expected comparable luminosities for gamma rays and neutrinos would require $\hat{\psi}_\nu \gtrsim 1$. This suggests that $D_1 \lesssim 1$, which allows to reach the energy limit of $\sim 10^{19}$ eV only for muon neutrinos from pion decay, and only for relatively high ratios of the energy in protons and magnetic fields compared to the energy in radiation (electrons). It should be noted that hadronic models can produce $\bar{\mathcal{L}}_\nu(\hat{\mathcal{E}}_\nu) \gtrsim \bar{\mathcal{L}}$ also for relatively moderate values of $\xi_{B\gamma}$, if $\mathcal{D} \approx \mathcal{D}^*$; then, the hadronic radiative efficiency (neutrinos + gamma rays) takes its maximum of about 50%, so that a comparable emission in neutrinos, high energy and low energy photons can be achieved for $\xi_{pB} \sim \xi_{B\gamma} 1$. This, however, leads to maximum neutrino energies much below the upper limits stated in Eqs. (40a) and (42a), so that, under realistic assumptions, flares from AGN jets should not be expected to emit considerable neutrino fluxes above a few times 10^{18} eV.

To get an estimate on event rates in current or planned VHE/UHE neutrino observatories, we consider the example of the May 7, 1997 flare of Mkn 501, which lasted 3×10^4 s: The total isotropized energy emitted in optical to X-ray photons of this flare is $\bar{\mathcal{L}} \sim 2 \times 10^{50}$ erg; taking the luminosity distance of ≈ 160 Mpc, and assuming $\bar{\mathcal{L}}_\nu \sim \bar{\mathcal{L}}$ as suggested by TeV observations, this corresponds to a total energy in neutrinos of $\hat{\mathcal{E}}_\nu \sim 10^{18}$ eV at earth of about 6×10^5 erg km $^{-2}$, which would produce $\sim 3 \times 10^{-7}$ neutrino induced showers per km 3 air volume. The biggest air fluorescence detectors currently planned would cover about 3×10^5 km 3 air, and the ground array of the Pierre Auger Observatory would correspond to about 5×10^3 km 3 , which would clearly be not sufficient to detect the neutrino emission of a single AGN flare. Following an $\mathcal{E}_\nu^{2/3}$ power spectrum, the total energy in neutrinos at $\mathcal{E}_\nu \sim 10^{15}$ eV would be about 6×10^3 erg km $^{-2}$, which would cause $\sim 3 \times 10^{-3}$ events in a 1 km 3 underwater/ice Cherenkov detector. Also here, even the biggest neutrino telescope currently considered would not be able to “see” single AGN flares. The best we can expect is therefore to collect diffuse fluxes corresponding to many AGN flares and determine the average properties of their neutrino spectra. The detailed knowledge of the time integrated emission spectra of AGN correlated transients, however, would still be necessary to determine reliable estimates for such diffuse fluxes.

B. Gamma ray bursts

Gamma Ray Bursts (GRBs), while not yet fully understood, are thought to be produced in highly relativistic outflows originating from a compact, explosive event over time scales of several seconds up to minutes [60,61]. Recent observations of GRB afterglows (e.g. [62] and references therein) indicate that they are located at cosmological distances, which requires a characteristic luminosity of about 10^{51} erg s $^{-1}$ under the assumption of isotropic emission. Possible scenarios which could release that much energy over the time scales observed are, e.g., the coalescence of a neutron star binary, or the collapse of a supermassive star. The radiation observed from GRBs is expected to be due mainly to synchrotron or inverse Compton radiation from relativistic electrons accelerated at shock fronts occurring near the interface of the expanding relativistic shell (*external shocks*), or at shocks forming within the unsteady outflow itself (*internal shocks*) [63]. The same mechanisms would also accelerate protons, which could reach energies of the order of the highest energy cosmic rays, $\sim 10^{20}$ eV [64]. Due to the interaction with the dense photon field in the burst, these protons can produce efficiently VHE and UHE neutrinos [13]. Neutrinos of lower energy may also be produced by pp interactions between cold protons in the colliding ejecta [12]. We examine here in more detail the spectrum and maximum energy of the neutrinos from $p\gamma$ interactions in internal shocks.

1. Cosmological fireball models and internal shocks

Many GRBs show intrinsic variability on time scales $\mathcal{T} \sim 10^{-3}$ –1 s (hereafter written as $\mathcal{T} \equiv [0.1 \text{ s}] \mathcal{T}_{-1}$, $10^{-2} < \mathcal{T}_{-1} < 10$), while the total burst durations are $\mathcal{T}_{\text{GRB}} \sim 10^{-2}$ – 10^3 s [60]. This implies that their energy is released in a volume of the typical dimension of compact or stellar objects, $R_0 \sim 10^7$ – 10^{10} cm. For a total energy of $\gtrsim 10^{52}$ erg, this leads to a local photon density

of $\gtrsim 10^{21} \text{ erg cm}^{-3}$ with photon energies $\gg m_e c^2$. These “fireballs” (and even much weaker ones as well) would be optically thick to $\gamma\gamma$ pair creation, and for small baryonic loads, $M_{\text{bar}} \gtrsim 10^{-6} M_\odot$, the expansion leads to a conversion of almost all the radiation energy into bulk kinetic energy of motion, accelerating to a limiting Lorentz factor of $\Gamma \sim \eta = \bar{E}_{\text{GRB}}/M_{\text{bar}} \gg 1$, before photons can escape [65]. Hence, a dissipation mechanism reconverting the bulk kinetic motion into radiation is required after the flow becomes optically thin: this can be achieved by electron acceleration at shock waves occurring when the ejecta run into external matter [65]. Moreover, internal shocks can form in the ejected wind if the outflow is non-steady, i.e. η varies significantly over time scales comparable to $\mathcal{T} \ll \mathcal{T}_{\text{GRB}}$, which can lead to faster shells catching up with slower shells [25], similarly to what was discussed for AGN in Sect. III A. These internal shocks can dissipate the kinetic energy with an efficiency comparable to external shocks. While external shocks are expected to produce a relatively featureless outburst over time scales comparable to the total burst duration, $\mathcal{T}_{\text{GRB}} \sim 10^{-2} - 10^3 \text{ s}$, internal shocks could be associated with the rapid variability within the burst on time scales down to milliseconds. In both external and internal shocks a substantial fraction of the gamma radiation is produced by synchrotron cooling of the shock-accelerated electrons.

The typical energy of the burst photons in the observers frame is $\varepsilon_{\text{b,GRB}} \sim 300 \text{ keV}$ [60]. In the comoving frame of the gas moving with a bulk Lorentz factor η the characteristic photon energy radiated by synchrotron cooling of electrons heated at a shock of relative Lorentz factor Γ_{sh} is $\langle \epsilon \rangle \sim [0.04 \text{ eV}] \xi_{ep}^2 \Gamma_{\text{sh}}^2 B_{\text{G}}$, where $\xi_{ep} = \bar{u}_e/\bar{u}_p$ is the energy density ratio of electrons to protons (ions) behind the shock wave [65]. For mildly relativistic internal shocks, $\Gamma_{\text{sh}} - 1 \sim 1$, this leads to $B \sim [2 \times 10^6 \text{ G}] \xi_{ep}^{-2} \eta^{-1}$. At the dissipation radius where internal shocks occur [25],

$$r_{\text{d}} \sim c \mathcal{T} \eta^2 \quad , \quad (43)$$

i.e. where the radiated gamma rays are produced, the comoving magnetic field energy density may be parametrized through $u_B = \xi_{B\gamma} u_{\text{ph}}$, so that

$$B \sim 10^{11} \text{ G} \times (\xi_{B\gamma} b_{\text{L}} \mathcal{L}_{51})^{1/2} \mathcal{T}_{-1}^{-1} \eta^{-3} \quad , \quad (44)$$

where $\mathcal{L}_{51} = \mathcal{L}/10^{51} \text{ erg s}^{-1}$ is the normalized GRB isotropic luminosity at the break energy in the observer frame, and b_{L} is the bolometric correction factor correlating this specific luminosity to the total gamma-ray luminosity of the burst. The value of b_{L} depends essentially on the high energy cutoff in the photon emission, which cannot be inferred from current data; for internal shocks one expects $< 10^{-1} \text{ GeV}$ in the comoving frame, corresponding to a canonical value $b_{\text{L}} \sim 10$. Comparing both expressions for the canonical luminosity and bolometric correction factor we obtain $B \sim [5 \times 10^3 \text{ G}] \xi_{B\gamma}^{-1/4} \xi_{ep}^{3/2} \mathcal{T}_{-1}^{1/2}$ and $\eta \sim 400 \xi_{B\gamma}^{1/4} \xi_{ep}^{-1/2} \mathcal{T}_{-1}^{-1/2}$. In the internal shock model, additional constraints on the bulk Lorentz factor can be inferred from the requirement that the dissipation radius is larger than the radius of the photosphere, $r_{\text{ph}} \sim [10^{18} \text{ cm}] \mathcal{L}_{51} \eta^{-3}$, below which the wind is optically thick, and the radius of the external termination shock, $r_{\text{xsh}} \sim [10^{18} \text{ cm}] \mathcal{L}_{51} \mathcal{T}_{\text{GRB}} \eta^{-2/3}$, which requires the bulk Lorentz factor of the ejecta, $\Gamma \sim \eta$, to be in the range $30 \lesssim \Gamma \lesssim 10^3$, assuming standard parameters. This is consistent with the values derived from the equipartition conditions, if $\xi_{ep} > 0.1$; this condition is also required by energetic considerations, since only the electrons convert their energy efficiently into radiation in the gamma ray band, and the total energy in the burst is in most scenarios limited to about 10^{52} erg . Models predicting the acceleration of UHECR protons at internal shocks in GRBs also need the parameters B and Γ in this regime [64,66].

We still need to relate the parameters R , x_{L} and \mathcal{D} , defined in Sect. III B for a causally connected emission region moving at some angle Θ_{view} to the line of sight, to the parameters describing the expanding flow in a GRB. In the comoving frame of the wind (at an arbitrary point), the apparent thickness of the wind zone extending to a radius r is r/Γ . Similarly, the transversal extent of causally connected regions in the comoving frame of the flow is r/Γ , because regions farther apart move away from each other with velocities larger than c (r/Γ may thus be interpreted as the “Hubble radius” of the expanding emission region, c.f. [65]). If the energy dissipation takes place at a radius r_{d} where the bulk Lorentz factor is saturated, $\Gamma \sim \eta$, the comoving “linear size” of the emission region can thus be written as $R \sim r_{\text{d}}/\eta$. On the other hand, the isotropic luminosity of the burst in the observer frame is related to the photon energy density in the comoving frame of the wind by $\mathcal{L} = 4\pi r_{\text{d}}^2 c \Gamma^2 u_{\text{ph}}$, which is identical to Eq. (13) in conjunction with the linear boosting formula, $\mathcal{L} = L \mathcal{D}^4$, if we use the parameters $R = r_{\text{d}}/\Gamma$, $x_{\text{L}} = 1$ and $\mathcal{D} = \Gamma$. For $\Gamma \sim \eta = \text{const}$, all parameters are therefore correctly derived if we treat the GRB as emission from a spherical region of radius $R \sim r_{\text{d}}/\eta$ boosted with a Doppler factor $\mathcal{D} \sim \eta$. Moreover, if the gamma ray emission originates from synchrotron radiation of electrons whose cooling time scale is much shorter than the crossing time [25], we can also apply $R \approx c \mathcal{T} \mathcal{D}$, or $\rho_{\text{T}} \approx 1$; note that \mathcal{T} is the variability time scale in the burst, *not* the burst duration. Since the radius R is the “Hubble radius” of the expanding emission region, we obviously also have $\beta_{\text{ex}} = 1$, and the effective space fraction available for the gyration of protons is essentially constrained by adiabatic losses, $\rho_{\text{L}} \sim (\pi \alpha \theta_{\text{F}})^{-1}$; as argued in Sect. IV A 2, some ambiguity arises from the unknown dependence of the magnetic field on R , i.e. whether it is isotropized by reconnection ($\alpha = 2$) or not ($\alpha = 1$).

2. GRB neutrino spectrum and maximum energy

The observed electromagnetic spectrum of a GRB can be approximately described as a broken power law, with a break energy $\varepsilon_{b,GRB} \sim 300$ keV in the observer frame. The photon number spectrum is then given by $N(\epsilon) \propto \epsilon^{-2}$ for $\epsilon > \epsilon_{b,GRB}$ (thus $a = 2$), and for $\epsilon < \epsilon_{b,GRB}$ it is $N(\epsilon) \propto \epsilon^{-2/3}$, with $\epsilon_{b,GRB} = \varepsilon_{b,GRB} \mathcal{D}^{-1}$. This yields a proton break Lorentz factor in the range $10^4 \lesssim \gamma_b \lesssim 5 \times 10^5$ for the range of possible Doppler factors given above. When we consider neutrinos of energy $\mathcal{E}_\nu \gtrsim 100$ TeV, we require proton Lorentz factors of $\gamma \gtrsim 3 \times 10^6 / \mathcal{D}$. For $\mathcal{D} \sim 100$, we therefore have $\gamma \gtrsim \gamma_b$; for simplicity, we restrict our considerations to the case $\gamma \gg \gamma_b$, noting that this might be only marginally correct for the lower energy bound of the VHE neutrino regime. In a $\epsilon^{-2/3}$ low energy spectrum, we simply have $N_{ph}/N_{ph,b} = 4 - 3(\gamma_b/\gamma)^{1/3}$ for $\gamma > \gamma_b$; in the following, we use $N_{ph}/N_{ph,b} \sim 3$ for all Lorentz factors under consideration. The coordinates of the star-point of the parameter space, i.e. where all proton cooling processes have equal time scales at the maximum proton energy, are then

$$\mathcal{D}^* \approx 1.2 \times 10^2 \times \mathcal{L}_{51}^{1/4} \mathcal{T}_{-1}^{-1/4} \quad (45a)$$

$$B^* \approx 4.5 \times 10^4 \text{ G} \times \mathcal{L}_{51}^{-1/6} \mathcal{T}_{-1}^{-1/2} \theta_F^{1/3} \quad (45b)$$

$$\xi_{B\gamma}^* \approx 0.68 \times \mathcal{L}_{51}^{1/6} \mathcal{T}_{-1}^{-1/2} \theta_F^{2/3} b_L^{-1} \quad (45c)$$

The bolometric correction factor is kept as a free parameter, using $b_L = 10$ for numerical estimates. In the following we express the magnetic field by its equipartition parameter, and introduce canonical units for the Doppler factor, $\mathcal{D}_2 = \mathcal{D}/100$. Fig. 2 shows the GRB parameter space and the separate regions of dominance of the various cooling processes limiting the neutrino energy. It also shows the corresponding neutrino spectral shapes, for canonical parameters $\theta_F = 1$, $\mathcal{L}_{51} = 1$, and a set of possible variability time scales; unlike in the AGN case, we do not use parameters scaled relative to the star-point, and put more emphasis on secondary particle cooling, which we consider separately for pions and muons. We see that in all cases, the energy of neutrinos from both pion and muon decay is limited by secondary particle cooling, where synchrotron cooling of pions and muons plays the most important role. Only in a limited part of the parameter space does an additional break due to adiabatic cooling of muons appear in the spectrum, while adiabatic cooling is generally unimportant for pions. At the star-point, the maximum neutrino energy from Gamma Ray Bursts is therefore considerably below $\hat{\mathcal{E}}_\nu^*$, so that we omitted it from Eqs. (45) to avoid confusion.

Because of the dominance of secondary particle cooling, Eqs. (30) must be used to determine the neutrino energy limit at a given Doppler factor, $\hat{\mathcal{E}}_\nu(\mathcal{D})$, which is reached along a line $\xi_{B\gamma} = \check{\xi}_{B\gamma, \text{syn}(\star)}^*(\mathcal{D}/\mathcal{D}^*)^5$ in the parameter space, with

$$\check{\xi}_{B\gamma, \text{syn}(\mu)}^* = 1.9 \times 10^{-3} \times \mathcal{L}_{51}^{1/4} \theta_F \mathcal{T}_{-1}^{-1/4} \quad (46a)$$

$$\check{\xi}_{B\gamma, \text{syn}(\mu)}^* = 1.4 \times 10^{-4} \times \mathcal{L}_{51}^{1/4} \theta_F \mathcal{T}_{-1}^{-1/4}. \quad (46b)$$

The total energy of an isotropic GRB fireball is often assumed to be $\overline{E}_{GRB} \lesssim 10^{52}$ erg, and the radiation is assumed to be emitted over a solid angle $\Omega \gg \mathcal{D}^{-2}$. While collimation is a distinct possibility, the evidence for it is not as obvious as in AGN and isotropic outflows are possible. Note also that the transients considered here are single, isolated radiation spikes in the GRB, corresponding to two colliding subshells in the internal shock scenario, rather than the whole burst. In the following we assume that $\overline{E}_T / b_L \mathcal{L}_b \mathcal{T} \sim \overline{E}_{GRB} / b_L \mathcal{L}_b \mathcal{T}_{GRB} \sim \mathcal{L}_{51}^{-1}$. Thus for the canonical isotropized luminosity the typically assumed total burst energy is usually exhausted by the (isotropized) emission in electromagnetic radiation over all frequency bands, and equally distributed over the individual flares. The assumption that comparable amounts of energy are present also in other channels, like magnetic fields or protons, therefore requires $\Omega_{4\pi} \equiv \Omega / 4\pi < 1$. With the assumption $\xi_{pB} \sim 1$ we can then write $\xi_{B\gamma, \text{max}} \sim \frac{1}{2} \Omega_{4\pi}^{-1} \mathcal{L}_{51}^{-1}$. From this we find

$$\hat{\mathcal{D}}_{\pi(2)} \approx 3.5 \times \Omega_{4\pi}^{-1/5} \mathcal{T}_{-1}^{-1/5} \theta_F^{-1/5} \quad (47a)$$

$$\hat{\mathcal{D}}_{\mu(2)} \approx 6.0 \times \Omega_{4\pi}^{-1/5} \mathcal{T}_{-1}^{-1/5} \theta_F^{-1/5} \quad (47b)$$

which means that we only need to discuss the case $\hat{\mathcal{D}}_\mu > \mathcal{D}^*$. We then obtain for the neutrino energy limit

$$\hat{\mathcal{E}}_{\nu, \pi}(\mathcal{D}_1) \approx 3.8 \times 10^{17} \text{ eV} \times D_2^{3/2} \mathcal{T}_{-1}^{1/2} \theta_F^{-1/2} < 3 \times 10^{18} \text{ eV} \times \Omega_{4\pi}^{-3/10} \mathcal{T}_{-1}^{1/5} \theta_F^{-4/5} \quad (48a)$$

$$\hat{\mathcal{E}}_{\nu, \mu}(\mathcal{D}_1) \approx 1.0 \times 10^{17} \text{ eV} \times D_2^{3/2} \mathcal{T}_{-1}^{1/2} \theta_F^{-1/2} < 1.5 \times 10^{18} \text{ eV} \times \Omega_{4\pi}^{-3/10} \mathcal{T}_{-1}^{1/5} \theta_F^{-4/5} \quad (48b)$$

It therefore seems that, for very narrow emission cones, $\Omega_{4\pi} \lesssim 10^{-2}$, and long flares, $\mathcal{T}_{-1} \sim 10$, photohadronic neutrinos from GRBs can reach energies up to 10^{19} eV and above. However, the corresponding normalized neutrino luminosities at the neutrino energy limit are

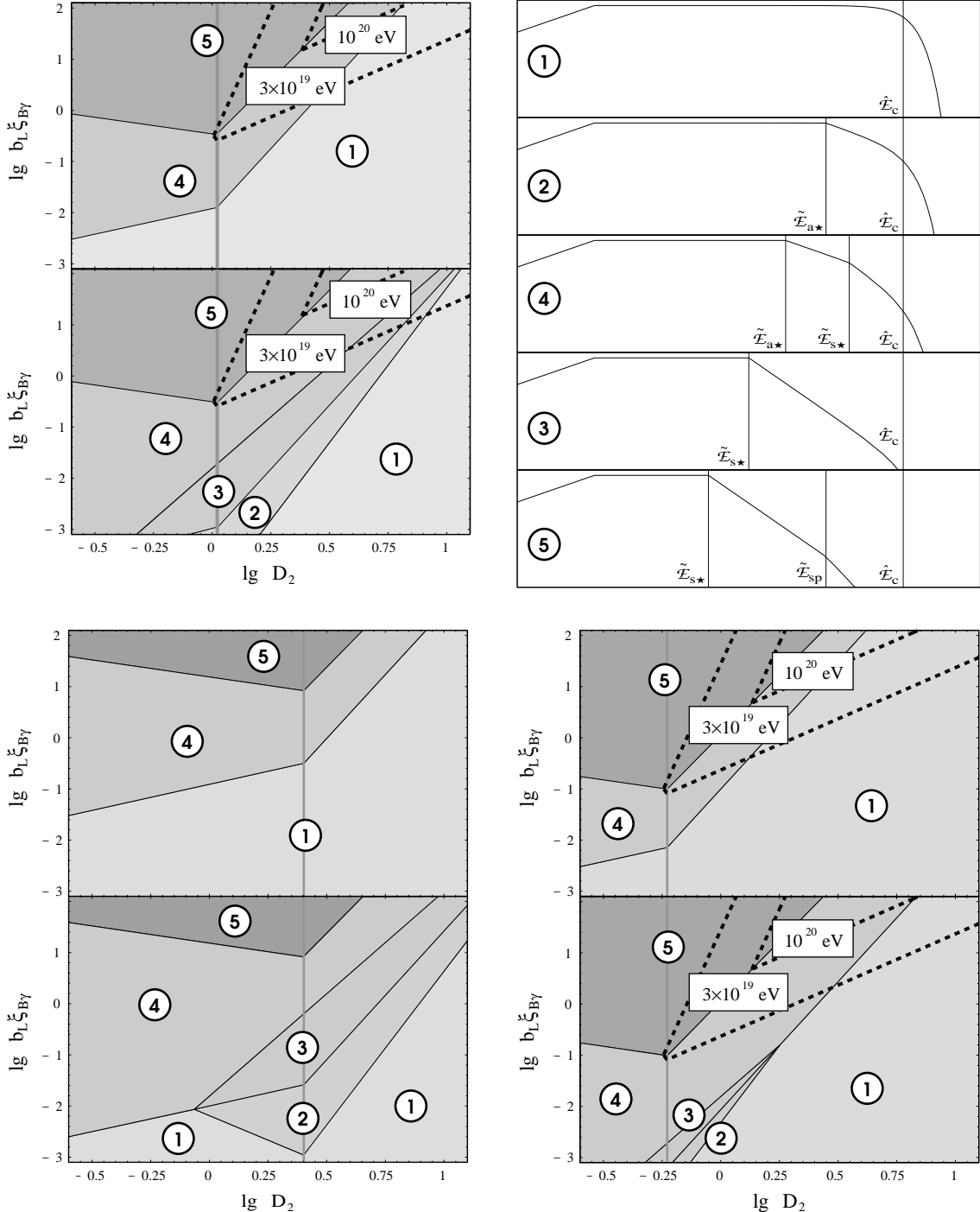


FIG. 2. Dominant cooling processes and spectral shapes for neutrino production in Gamma Ray Bursts — **Upper left and lower panel:** Parameter space for three different variability time scales T and canonical values of the other parameters (see text). Shaded regions correspond to spectral shapes produced by the overlay of different cooling processes for protons and secondary particles. In each figure, the upper part corresponds to neutrinos from pion decay and the lower part for neutrinos from muon decay. The central line divides regions where the proton maximum energy is determined by photohadronic cooling (left from the line) and adiabatic cooling (right from the line), except in region (5), where synchrotron cooling is the limiting process. Other regions indicate the effect of secondary particle cooling: (1) no effect, (2) $\dot{\mathcal{E}}_{\nu,ad(*)} < \dot{\mathcal{E}}_{\nu}$, (3) $\dot{\mathcal{E}}_{\nu,ad(*)} < \dot{\mathcal{E}}_{\nu,syn(*)} < \dot{\mathcal{E}}_{\nu}$, (4) $\dot{\mathcal{E}}_{\nu,syn(*)} < \dot{\mathcal{E}}_{\nu}$, (5) $\dot{\mathcal{E}}_{\nu,syn(*)} < \dot{\mathcal{E}}_{syn(p)} < \dot{\mathcal{E}}_{\nu}$. **Upper right:** Schematic representation of corresponding spectral shapes (time integrated power per logarithmic interval of energy), $\log \bar{\mathcal{L}}_{\nu}(\mathcal{E}_{\nu})$ vs. $\log \mathcal{E}_{\nu}$. The lower break indicates the spectral change at about 100 TeV due to the change of the photon target spectrum at $\gamma_p \sim \gamma_b$ (see Ref. [13]), which is not discussed in this paper.

$$\hat{\psi}_{\nu,\pi}(\mathcal{D}_1) \approx 7 \times 10^{-6} \times D_2 \theta_F < 3 \times 10^{-5} \times \Omega_{4\pi}^{1/5} \mathcal{T}_{-1}^{-1/5} \theta_F^{4/5} \quad (49a)$$

$$\hat{\psi}_{\nu,\mu}(\mathcal{D}_1) \approx 5 \times 10^{-7} \times D_2 \theta_F < 3 \times 10^{-6} \times \Omega_{4\pi}^{1/5} \mathcal{T}_{-1}^{-1/5} \theta_F^{4/5}, \quad (49b)$$

which shows that even in the limiting case $\mathcal{D} = \hat{\mathcal{D}}$ only very small fractions of the photon energy can be emitted in neutrinos at the limiting energy. Since we assumed $\xi_{pB} \sim 1$ and $\xi_{B\gamma,\max} \sim 1$ in our calculations, the low values of $\hat{\psi}_\nu$ are clearly due to a very low efficiency along the line $\xi_{B\gamma} = \xi_{B\gamma,\text{syn}(\star)}(\mathcal{D})$. Assuming a neutrino conversion efficiency of $\zeta_\nu \sim 0.2$, $\xi_{B\gamma} \sim 1$ and $u_p \sim 5\epsilon_b^2(dN_{\text{ph}}/d\epsilon)_b$ (which is consistent with our assumption $\xi_{pB} \sim \xi_{B\gamma} \sim 1$ if we consider $b_L \sim 10$), Waxman and Bahcall [13] derived a GRB-related neutrino event rate at $\mathcal{E}_\nu \gtrsim 10^{14}$ eV of about 10–100 per year in a km^3 detector. This event rate would be below the expected background, but still statistically significant because of the time and directional correlation to the bursts. It is clear from the above that if we try to maximize the neutrino energy in the UHE range, following Eq. (48), this estimate would have to be reduced by more than 4 orders of magnitude, leading to insignificant event rates at these highest energies even if the usually larger detector volume of UHE experiments is taken into account.

We can also turn the question around and ask which is the region of parameter space where neutrino fluxes of the magnitude predicted by Waxman and Bahcall [13] are expected, and then derive the maximum neutrino energy for these parameters, considering secondary particle cooling. The assumptions of Waxman and Bahcall for a single burst (or sub-flare) can be essentially put in the form $\mathcal{L}_\nu \sim 0.2 \mathcal{L}_b \mathcal{T}$, which can be rewritten in the form of Eq. (49) as $b_L \zeta_\nu \xi_{B\gamma} \xi_{pB} \sim 0.2 A_s$; for $A_s \sim b_L$ the condition for obtaining neutrino fluxes of this magnitude or larger can thus be written as $\xi_{pB} \xi_{B\gamma} \gtrsim (\mathcal{D}/\mathcal{D}^*)^4$. Fig. 2 shows that this region is entirely enclosed by the regions of pion, muon and proton synchrotron cooling dominance. Considering $\hat{\mathcal{E}}_{\nu,\text{syn}(\star)}$ as the relevant cutoff energy of the neutrino spectrum, inserting into Eq. (20) we obtain

$$\hat{\mathcal{E}}_{\nu,\pi} < 2.3 \times 10^{16} \text{ eV} \times \mathcal{D}_2^2 \mathcal{T}_{-1}^{1/2} < 2.1 \times 10^{16} \text{ eV} \times \xi_{pB}^{1/2} \mathcal{L}_{51}^{1/2} \Omega_{4\pi}^{-1/2} \quad (50a)$$

$$\hat{\mathcal{E}}_{\nu,\mu} < 2.7 \times 10^{15} \text{ eV} \times \mathcal{D}_2^2 \mathcal{T}_{-1}^{1/2} < 2.5 \times 10^{15} \text{ eV} \times \xi_{pB}^{1/2} \mathcal{L}_{51}^{1/2} \Omega_{4\pi}^{-1/2} \quad (50b)$$

where the second limit was derived using $\xi_{B\gamma} < \frac{1}{2} \Omega_{4\pi}^{-1} \mathcal{L}_{51}^{-1}$. For the canonical assumption $\xi_{pB} \sim 1$, we see that $\Omega_{4\pi} \ll 1$ would be required for Gamma Ray Bursts to produce UHE neutrinos with considerable fluxes. We note that this result is due to the effects of synchrotron cooling of pions and muons — disregarding this effect would strongly overestimate the maximum neutrino energy.

It has also been proposed that UHE protons may be produced at external shocks [67]. One uncertainty here is that it has not yet been quantitatively shown that the standard relations valid for first order Fermi acceleration apply to shock waves of such high Lorentz factors ($\Gamma \sim 10^3$). Disregarding this problem, and assuming that a considerable fraction of the gamma ray emission is also produced at the external shock — which is possible for bursts where the γ -ray light curve is smooth, or has a smooth component underlying a few spikes or low amplitude spikes — our considerations would apply also to this scenario if we set $\mathcal{T}_{-1} \sim 10-10^3$. If we require that neutrino fluxes comparable to the gamma ray flux are produced, Eq. (50) applies unchanged; we note that its upper limit is independent of the variability time scale, and thus applies to internal and external shocks in the same way. Again, synchrotron cooling of secondary particles is the relevant limiting process for the neutrino energy.

3. The relation between cosmic ray and neutrino maximum energies

GRBs have been proposed as possible sources for the highest energy cosmic rays [64], which are observed up to $\hat{\mathcal{E}}_p \sim 3 \times 10^{20}$ eV [20]. The maximum proton energy in the observer frame is $\hat{\mathcal{E}}_p = m_p c^2 \hat{\gamma}_p \mathcal{D}$; at the star-point of the parameter space, we find $\hat{\mathcal{E}}_p^* \approx 4 \times 10^{19} \mathcal{L}_{51}^{1/3} \theta_F^{-2/3}$. The highest proton energy for a given Doppler factor is obviously achieved at the line of equal time scales for proton synchrotron colling and adiabatic losses (the same condition which determines the maximum neutrino energy if secondary particle cooling plays no role). This is the border line of region (5) in the parameter space shown in Fig. 2, so we find $\hat{\mathcal{E}}_p = \hat{\mathcal{E}}_p^* (\mathcal{D}/\mathcal{D}^*)^{4/3}$ for $\mathcal{D} \geq \mathcal{D}^*$, leading to

$$\hat{\mathcal{E}}_p(\mathcal{D}_2) \approx 3.5 \times 10^{19} \text{ eV} \times \mathcal{D}_2^{4/3} \mathcal{T}_{-1}^{1/3} \theta_F^{-2/3} \quad (51)$$

Since $\xi_{B\gamma} \propto \mathcal{D}^{14/3}$ along this line, the required magnetic field equipartition parameter rises fast; as a function of the proton energy in the observers frame, $\hat{\mathcal{E}}_{p,20}$, in units of 10^{20} eV, we can formulate the minimum requirements in \mathcal{D} and $\xi_{B\gamma}$ as

$$\xi_{B\gamma,\text{UHE}}(\hat{\mathcal{E}}_{p,20}) > 1.3 \hat{\mathcal{E}}_{p,20}^{7/2} \mathcal{T}_{-1}^{-1/2} \theta_F^{34/9} \mathcal{L}_{51}^{-1} \quad (52a)$$

$$\mathcal{D}_{\text{UHE}}(\hat{\mathcal{E}}_{p,20}) > 2.2 \hat{\mathcal{E}}_{p,20}^{3/4} \mathcal{T}_{-1}^{-1/4} \theta_F^{1/2} \quad (52b)$$

In correspondence with the result of Waxman [64], we find that bulk Lorentz factors $\mathcal{D} \gtrsim 300$ and magnetic fields close to equipartition with the radiation are required to produce $\hat{\mathcal{E}}_p \gtrsim 1$, provided that protons are accelerated on their Larmor time scale.

However, to reach values $\hat{\mathcal{E}}_{p,20} > 3$, which would be necessary to explain also the highest energy events seen in air shower arrays, the demands on $\xi_{B\gamma}$ increase strongly, requiring $\Omega_{4\pi} \ll 1$ even for bursts without short variability.

Assuming optimal conditions for the production of UHE cosmic rays, i.e. $\mathcal{D} = \check{\mathcal{D}}_{\text{UHE}}(\hat{\mathcal{E}}_{p,20})$ and $\xi_{B\gamma} = \check{\xi}_{B\gamma,\text{UHE}}(\hat{\mathcal{E}}_{p,20})$, we can derive the corresponding maximum neutrino energy as a function of $\hat{\mathcal{E}}_{p,20}$ as

$$\hat{\mathcal{E}}_{\nu,\pi} \Big|_{\hat{\mathcal{E}}_p = \hat{\mathcal{E}}_p(\mathcal{D})} \approx 4.8 \times 10^{17} \text{ eV} \times \hat{\mathcal{E}}_{p,20}^{5/4} \theta_{\text{F}}^{1/9} \mathcal{T}_{-1}^{1/4} \quad (53a)$$

$$\hat{\mathcal{E}}_{\nu,\pi} \Big|_{\hat{\mathcal{E}}_p = \hat{\mathcal{E}}_p(\mathcal{D})} \approx 4.2 \times 10^{16} \text{ eV} \times \hat{\mathcal{E}}_{p,20}^{5/4} \theta_{\text{F}}^{1/9} \mathcal{T}_{-1}^{1/4} \quad (53b)$$

where we again use $\hat{\mathcal{E}}_{\nu,\text{syn}(\star)}$ as the limiting energy. For $\mathcal{D} > \check{\mathcal{D}}_{\text{UHE}}(\hat{\mathcal{E}}_{p,20})$, the production of cosmic rays with $\geq \hat{\mathcal{E}}_{p,20}$ is possible in a conical region of the parameter space, as shown in Fig. 2. However, one can easily see that, considering the constraint $\xi_{B\gamma} \lesssim \frac{1}{2} \Omega_{4\pi}^{-1} \mathcal{L}_{51}^{-1}$, and requiring a neutrino luminosity comparable to the gamma ray luminosity, $\bar{\mathcal{L}}_{\nu} \sim \bar{\mathcal{L}}$, the maximum neutrino energy corresponding to $\mathcal{E}_p \gtrsim 10^{20} \text{ eV}$ cannot deviate much from the value given in Eqs. (53). Thus, although secondary particle cooling keeps the maximum neutrino energy much below the maximum proton energy, $\hat{\mathcal{E}}_{\nu}$ still increases with $\hat{\mathcal{E}}_p$, so that an observed cutoff in the neutrino flux correlated with a Gamma Ray Burst imposes an upper limit on the maximum proton energy as well. If GRBs indeed produce cosmic rays up to the highest observed energies, we would expect that the muon neutrino spectrum (from pion decay) extends to about 10^{18} eV , and that the electron neutrino component cuts off about one order of magnitude below this energy. Comparison with Eq. (50) shows that this would be incompatible with high neutrino flux levels, unless extreme parameters for the collimation and proton content of Gamma Ray Bursts, i.e. $\Omega_{4\pi} \ll 1$ and/or $\bar{\xi}_{pB} \gg 1$, are assumed.

Assuming “standard” parameters, we therefore would have to conclude that Gamma Ray Bursts, as currently understood, are unlikely to be *both* the sources of considerable neutrino fluxes *and* of the highest energy cosmic rays. However, this possibility cannot be excluded a priori, and it is important to point out that the search for GRB correlated VHE *and* UHE neutrinos could test this hypothesis experimentally. Depending on the result of this search, we would be led to one of the following conclusions: (A) If GRB correlated VHE neutrino fluxes on the level predicted by Waxman and Bahcall [13] could be established, but UHE neutrino experiments would not find a corresponding flux at $\mathcal{E}_{\nu} \gtrsim 10^{17} \text{ eV}$, this would show that GRBs have a strong content of energetic protons, which however do not exceed energies in the observers frame of a few times 10^{19} eV . This would point to a different origin of the highest energy cosmic rays. (B) If GRB correlated neutrinos are neither in the VHE nor in the UHE regimes, GRB might still contain large amounts of energetic protons, which could even reach energies $\gtrsim 10^{20} \text{ eV}$. However, the hypothesis that this makes Gamma Ray Bursts the dominant source of UHE cosmic rays might still be problematic if most of these protons are confined in the expanding shell, and suffer considerable adiabatic losses before they can be ejected as cosmic rays. The most obvious way to circumvent this problem is neutron production and subsequent decay into protons [66], which would be associated with neutrino production. Low neutrino fluxes would prove that the efficiency for this process is small, so that probably most of the cosmic ray energy in Gamma Ray Burst would be reconverted into bulk kinetic motion. (C) Finally, if strong GRB correlated neutrino fluxes both in the VHE and UHE regime are measured, this would corroborate the hypothesis that GRBs are indeed the dominant source of UHE cosmic rays. At the same time, it would impose severe constraints on the GRB parameters; e.g., it would provide strong evidence that GRB outflows are collimated into narrow cones, $\Omega_{4\pi} \ll 1$.

V. CONCLUSIONS

We have presented a detailed investigation of the production processes of very energetic ($\gtrsim 10^{14} \text{ eV}$) photohadronic neutrinos in relativistically boosted astrophysical sources. Using the constraints set by the source variability, and assuming that the acceleration process for protons is of the Fermi type, we derived limits on the maximum energy and the position of possible breaks in the neutrino spectrum. Comparing the effects of various cooling processes for both protons and secondary particles in the hadronic cascade leading to neutrino production (i.e. pions and muons), we find a general upper limit on the neutrino maximum energy, which does only depend on the Doppler factor of the emission region relative to the observer. Energetic constraints allow one to turn this into a general upper limit, which is only dependent on observational parameters of the transient, but not on any model dependent parameters. This is the major result of this paper. In some cases, and assuming that the energy in protons, magnetic field and photons are near equipartition, stricter limits can be imposed when considering both neutrino energy and expected flux. We apply this general result to two classes of proposed cosmic neutrino sources: hadronic models of Doppler beamed jets from Active Galactic Nuclei (AGN), also called blazars, which are known to emit most of their energetic radiation in short, distinct flares, and Gamma Ray Bursts.

For blazar flares, we confirm that under the most common assumptions the neutrino energy is limited to $\lesssim 10^{18} \text{ eV}$ by Larmor radius (or adiabatic) constraints of the accelerated protons. For short ($\lesssim 1 \text{ hrs}$) flares, however, the maximum energy of neutrinos from muon decay may be additionally suppressed by muon synchrotron cooling. Assuming that the AGN is fueled by Eddington

limited accretion on a supermassive Black Hole with $M_{\text{BH}} \leq 10^{10} M_{\odot}$, we show that neutrinos from AGN flares cannot exceed energies of $\sim 10^{19}$ eV, independently of the time scale of the flare. For electron neutrinos, which result only from muon decay, we can show that fluxes of the magnitude usually assumed in the literature (i.e. similar to the X-ray luminosity of the source) can only be attained if the energy extends only up to about 10^{18} eV. Unless vacuum neutrino oscillations occur in nature, this has important implications for the neutrino event rates expected in the Pierre Auger Observatory, where electron neutrinos are proposed to be most easily detected because of the distinct properties of their induced air showers.

For Gamma Ray Bursts (GRBs), we find that the synchrotron cooling of pions and muons limits the maximum neutrino energy over most of the allowed region of parameter space. We show that neutrinos from GRBs are very unlikely to exceed 10^{19} eV, regardless of whether they are produced in internal or external shocks. However, if we require that neutrinos are also produced with fluxes similar to the γ -ray flux, and applying the usual energetic constraints for near-isotropic GRB sources, we find an upper limit on the neutrino energy below $\sim 10^{17}$ eV for muon neutrinos, and below $\sim 10^{16}$ eV for electron neutrinos. This limit can only be increased to UHE ($> 10^{17}$ eV) neutrino energies if strongly collimated outflows, and/or a hadronic energy content clearly above equipartition with both magnetic field and radiation are assumed. On the other hand, we show that the hypothesis that GRBs accelerate protons up to the highest energies observed in cosmic ray air shower experiments ($\sim 3 \times 10^{20}$ eV) implies a flat neutrino power spectrum extending up to $\sim 10^{18}$ eV (without predicting the neutrino flux). This allows only two possibilities: (a) the hypotheses that (i) GRBs produce the highest energy cosmic rays and (ii) GRBs supply VHE neutrino fluxes comparable to their γ -ray flux are mutually exclusive, or (b) GRBs produce a measurable flux of UHE neutrinos, which would, if detected, show that they are indeed the dominating source of UHE cosmic rays, and thereby impose strong constraints on their physical properties.

As a corollary of our investigation of the relevance of secondary particle cooling to hadronic cascades in common models of astrophysical transients, we have also checked the effect of this process on other proposed, non-transient sources for cosmic neutrinos. In particular the predicted diffuse neutrino background from AGN cores, frequently used for event estimates in high energy neutrino detectors, was previously derived disregarding secondary particle cooling. Here we obtain for energies above 10^{15} eV a strongly reduced contribution and a lower cutoff in the electron neutrino component, and a reduction of about a factor 3 for the expected diffuse muon neutrino flux (see Appendix D).

In cosmic sources where the neutrino energy is limited by secondary particle cooling, which is clearly predicted for Gamma Ray Bursts and is possible in some blazar flares, the expected difference in the cutoff energy of electron and muon neutrinos could also serve as a laboratory to test the existence of neutrino vacuum oscillations in nature at very high energies — a detected change in the neutrino composition near the cutoff energy could rule out this possibility. Such a measurement would require a large detector sensitive in the range between $\sim 10^{15}$ and $\sim 10^{18}$ eV, capable of detecting both electron and muon neutrinos and able to distinguish between flavors.

ACKNOWLEDGMENTS

We wish to thank Karl Mannheim and Enrique Zas for helpful discussions during the preparation of the manuscript. This work was supported in part by the NASA under grant NAG5-2857.

APPENDIX A: PHOTOHADRONIC INTERACTIONS

The major photohadronic interaction channels on protons are single pion production with and without isospin flip, $p\gamma \rightarrow n\pi^+$ and $p\gamma \rightarrow p\pi^0$, followed by several two-pion production channels, and multi-pion production which dominates at very high interaction energies. Secondary neutrons can contribute negative pions from $n\gamma \rightarrow p\pi^-$ reactions, which are otherwise only produced in two-pion and multi-pion channels. The subsequent decay of the pions leads to neutrino production by

$$\pi^\pm \rightarrow \mu^\pm \nu_\mu (\bar{\nu}_\mu) \quad (\text{A1a})$$

$$\mu^\pm \rightarrow e^\pm \bar{\nu}_\mu \nu_e (\nu_\mu \bar{\nu}_e) \quad . \quad (\text{A1b})$$

The charge of the initial pion is only relevant for the $\nu : \bar{\nu}$ ratio; it plays a role for the electron neutrino component at energies $\mathcal{E}_\nu \approx 6 \times 10^{15}$ eV, where the detectability of $\bar{\nu}_e$ is enhanced due to the Glashow-Weinberg resonance in interaction with atmospheric electrons. Otherwise, neither underwater/ice, nor air shower experiments can distinguish between neutrinos and anti-neutrinos, so that we can disregard the sign of the pion charge. The average energy of the neutrinos is determined by decay kinematics: it can be written as $\langle E_\nu \rangle = E_{\nu,*}^{\text{RF}} \gamma_*$, where $E_{\nu,*}^{\text{RF}}$ is the energy of the neutrino in the rest frame of the decaying particle moving with γ_* (see Sect. III C for notational conventions). For pion decay, $E_{\nu,\pi}^{\text{RF}} = 30$ MeV [36], while in the three particle decay of the muon $\langle E_{\nu,\mu}^{\text{RF}} \rangle \approx \frac{1}{3} m_\mu c^2 = 35$ MeV. As an approximation, we may use $\langle E_{\nu,*}^{\text{RF}} \rangle \approx \frac{1}{4} m_\pi c^2$.

At low interaction energies, the photohadronic cross section is dominated by the $\Delta(1232)$ resonance, leading to single pion production with a $\pi^+ : \pi^0$ ratio of 1 : 2 and $E_\pi \approx 0.2E_p$; these relations are often used as characteristic for pion production, and we call it the Δ -approximation [68,2]. This approximation is in fact good for π^0 production, but less applicable to charged pion production: here s -wave production of charged pions strongly dominates at threshold over the wing of the Δ -resonance, and in the second resonance region, N^* resonances produce predominantly charged pions, making their effective cross section comparable to the $\Delta(1232)$ [69]. In the generic astrophysical “neutrino factory”, a proton spectrum extending up to a maximum energy $\hat{E}_p = m_p c^2 \gamma_p$, interacts with an isotropic power law photon distribution, $dN_{\text{ph}} \propto \epsilon^{-a} d\epsilon$, $a > 1$, extending] from a break energy ϵ_b to some cutoff at $\hat{\epsilon} \gg \epsilon_b$, with a total number density, $N_{\text{ph},b}$, of photons with $\epsilon > \epsilon_b$. (Of course, the background spectrum may contain thermal components, or may be a multiply broken power law, e.g. in the cores of AGN, which introduces further complications. However, many basic results can be obtained by the simple power law approximation). Below the break energy, we assume that the photon number spectrum is flatter than ϵ^{-1} everywhere. We can then define the inelasticity weighted effective cross section for pion production,

$$H_a = 2 \frac{a-1}{a+1} \int_1^\infty dx x^{-a} \sum_i \left[\kappa_i \sigma_i \right]_{\epsilon=x\epsilon_{\text{th}}^{\text{RF}}}^{\text{RF}} \quad \text{for } a > 1, \quad (\text{A2})$$

where $\epsilon_{\text{th}}^{\text{RF}} \approx 145$ MeV is the threshold photon energy for pion production in the proton rest frame, σ_i is the cross section, and $\kappa_i = \langle \Delta E_p / E_p \rangle_i$ is the proton inelasticity of the reaction channel, evaluated at a photon energy $\epsilon = x\epsilon_{\text{th}}^{\text{RF}}$ in the proton RF (see [69] for details). We disregard the upper cutoff in the photon spectrum, which is justified if the spectrum for $\epsilon < \epsilon_b$ is sufficiently steep; for spectra with $a < 2$, this approach is valid only in a limited range of Lorentz factors below γ_b . As a numerical approximation we may use $H_a \approx H_2/(a-1)$ for $1.5 < a \lesssim 3$, with $H_2 \simeq 22 \mu\text{barn}$. Introducing the characteristic Lorentz factor $\gamma_b = \epsilon_{\text{th}}^{\text{RF}}/2\epsilon_b$ of the protons, which is necessary to boost background photons at the break energy above the reaction threshold for pion production, we can then write the cooling time of protons with $\gamma_p = \gamma_b$ as $t_{b,\pi} \simeq [cN_{\text{ph},b} H_a]^{-1}$, where $N_{\text{ph},b}$ is the number density of photons with $\epsilon > \epsilon_b$; as a function of γ_p the cooling time $t_{p,\pi}$ is then expressed by Eqs. (5). If $\gamma_p \gg \gamma_b$, photohadronic interactions majorly happen at proton rest frame energies far above the threshold, where the cross section and efficiency is approximately constant; this justifies the approximation $t_{p,\pi} \approx [cN_{\text{ph}} H_2]^{-1}$, used throughout the paper.

If no other cooling processes apply, the average number of pions produced per proton can be found as $\langle N_\pi / N_p \rangle = \Pi_a / H_a \approx 7$, for $1.5 < a \leq 3$, where Π_a is defined as in Eq. (A2) by replacing the proton inelasticity by the pion multiplicity of the reaction channel. The average energy carried by each pion is then, independent of γ_p , given by $\langle E_\pi \rangle / E_p \approx \frac{1}{7} \approx m_\pi / m_p$; thus the Lorentz factor can be treated as conserved in the interaction, $\gamma_\pi^{\text{pr}} \approx \gamma_p$; here, γ_π^{pr} is the pion Lorentz factor *at production*, which has to be distinguished from γ_π^{dc} , the pion Lorentz factor *at decay*. For both pions and muons we consider the possibility that they lose energy during their lifetime, and thus $\gamma_\pi^{\text{dc}} < \gamma_\pi^{\text{pr}}$. Because of the small mass difference between pion and muon, we can also approximate $\gamma_\mu^{\text{pr}} \approx \gamma_\pi^{\text{dc}}$.

Distinguishing between the charged pion and neutral pion multiplicity in the definition of Π_a yields the charged pion fraction, $\pi^\pm : \pi^0 \approx 2 : 1$, almost independent of the power law index a [69]. This result includes all reaction channels, and is in contrast to the often used ratio $\pi^\pm : \pi^0 = 1 : 2$, which is derived from the Δ -approximation. The discrepancy of a factor of 4 emphasizes the importance of charged pion production away from the Δ -resonance in power law target photon spectra, which is also relevant for the kinematics: it explains the difference of the usual assumption, $\langle E_\pi \rangle \approx \frac{1}{5} E_p$, (which is strictly valid for π^0 production, see above) and our result for charged pion production, $\langle E_\pi \rangle \approx \frac{1}{7} E_p$.

APPENDIX B: SENSITIVITY RANGE AND ENERGY DEPENDENCE OF NEUTRINO DETECTOR TECHNIQUES

The low detection probability for neutrinos above the TeV range requires large detector volumes, which can be achieved e.g. by the extension of classical water Cherenkov detectors to larger dimensions, such as the NESTOR or Lake Baikal (and the recently cancelled, pioneering DUMAND) experiments, and similar projects in the planning stage [2]. The same technique is also efficient in the deep antarctic ice, as shown impressively by the recent detection of the first neutrino events by the AMANDA experiment [70], and there is hope to extend this detector to an effective volume of 1 km^3 in the future [71]. A cost-efficient way to further increase the detector volumes could be the detection of radio pulses [72] or acoustic waves [73] from neutrinos in water or ice, which however are limited to very high energies to obtain a reasonable signal-to-noise ratio [2].

The neutrino event rate per logarithmic energy interval in a given detector, $\phi_{\nu,\text{det}}$, can be written as the product of the neutrino *number* flux, $\bar{\mathcal{L}}_\nu / \mathcal{E}_\nu$, times the detection probability, $P_{\nu,\text{det}}$. For deep underwater or deep ice Cherenkov detectors, which are most efficient to detect muons from $\nu_\mu \rightarrow \mu$ conversions because of the large mean free path of muons in matter, the detection probability is essentially proportional to the ratio of the muon mean free path to the neutrino mean free path, yielding $P_{\nu,\text{det}} \propto \mathcal{E}_\nu^{0.8}$ for $\mathcal{E}_\nu \gtrsim 10^{12} \text{ eV}$. At energies above $\sim 10^{14} \text{ eV}$ the effective solid angle covered by the experiment is reduced by earth shadowing effects [74], so that this technique becomes ineffective for ultra high energies; it is also less sensitive to electron neutrinos, because the short range of the electron in matter reduces the effective volume. Radio Cherenkov detectors

are proposed to work best in deep ice. The detection probability is usually expressed as the effective volume of the detector, increasing as $P_{\nu,\text{det}} \propto \mathcal{E}_{\nu}^{1.5}$ for $\mathcal{E}_{\nu} \lesssim 10^{16}$ eV, and is roughly constant above 10^{16} eV [72]. The energy threshold for this technique is set by signal-to-noise constraints at $\sim 5 \times 10^{15}$ eV [2], thus in the relevant sensitivity range the detection probability can be treated as approximately constant. No clear predictions exist about the efficiency of the acoustic method yet, which is probably most interesting at ultra high energies.

Cosmic neutrinos may also cause air showers similar to cosmic rays, but deeper penetrating and thus distinguishable due to their large zenith angle [35]. At $\sim 10^{15}$ eV, such “horizontal” air showers are dominantly caused by atmospheric muons rather than cosmic neutrinos. Above 10^{17} eV, however, the atmospheric background becomes low, and the air scintillation technique used e.g. in the HiRes Fly’s Eye detector [75] or the Telescope Array [76], largely improves the detectability of horizontal air showers, providing much larger detection volumes than underground detectors. Above $\sim 10^{19}$ eV, the planned Pierre Auger Observatory [77] is expected to achieve considerable event rates, using the same technique in conjunction with ground arrays for particle detection [11]. The main caveat of the technique is the large atmospheric background — horizontal air showers produced by muon neutrinos can be easily confused with air showers from atmospheric muons generated by the prompt decay of charmed particles [35,2]. Horizontal air showers produced by electron neutrinos have the unique property to be mixed hadronic and electromagnetic showers [35], which allows to determine distinctive triggering criteria for hybrid detectors like the Pierre Auger Observatory, reducing the background [11]. This makes electron neutrinos most interesting for UHE neutrino astronomy.

The detection probability for deeply penetrating horizontal air showers can be expressed as the product of the hadronic neutrino cross section, $\sigma_{\nu p}$, and the detector acceptance for an horizontal air shower. Models predict correspondingly that $\sigma_{\nu p} \propto \mathcal{E}_{\nu}^{0.5}$ for $\mathcal{E}_{\nu} \gtrsim 10^{15}$ eV [78]. The detector acceptance for the Pierre Auger Observatory has been calculated as $\propto \mathcal{E}_{\nu}^{0.3}$ for $\mathcal{E}_{\nu} \gtrsim 10^{17}$ eV, where horizontal air shower detection is expected to be more efficient than other techniques [11]. This gives rise to $P_{\nu,\text{det}} \propto \mathcal{E}_{\nu}^{0.8}$, which is the same dependence as in the case in water/ice Cherenkov experiments. For other air shower experiments, the dependence of the shower acceptance on energy might be different, but a slow rise in the UHE regime seems to be a common feature.

The expressions for the energy dependence of the detection probability are highly approximate; exact results require expensive Monte-Carlo simulations, considering the detailed properties of the experiment. However, we note that the neutrino event rate per logarithmic energy interval, evaluated for the most common detector techniques, follows closely the neutrino power spectrum, $\phi_{\nu,\text{det}}/\mathcal{L}_{\nu} \sim \text{const}$. An exception is only the range between 10^{15} eV and 10^{17} eV, where horizontal air shower observations are still dominated by the atmospheric background and underground experiments affected by earth shadowing.

APPENDIX C: TIME SCALES FOR FERMI ACCELERATION

The time scale for first order Fermi acceleration at parallel shock fronts (defined as having the flow direction parallel to the magnetic field lines, with perpendicular and oblique shocks defined accordingly) is given by [29]

$$t_{\text{acc}} = \frac{\chi}{\chi - 1} \frac{r_{\text{L}}}{c\beta_{\text{sh}}^2} (y_1 + \chi y_2) \quad , \quad (\text{C0a})$$

where y_1 and y_2 are the ratios of diffusion coefficients parallel to the magnetic field, K_{\parallel} , taken in the regions upstream and downstream from the shock, respectively, to the Bohm diffusion coefficient, i.e. $y = 3K_{\parallel}/r_{\text{L}}c \leq 1$. The shock compression ratio, χ , satisfies $\chi \leq 4$ in nonrelativistic shocks, and is $\chi \approx 7$ in ultra-relativistic shocks. Assuming $y_2 \sim y_1 \equiv y$, we find $\theta_{\text{F}} \sim \beta_{\text{sh}}^{-2}y$. For parallel shocks, there is no upper limit on the value of y , which can be interpreted as a measure for the strength of the turbulence in the magnetic field, $y \approx (B/\delta B)^2$. In perpendicular shocks, one can show that $\theta_{\text{F}} \sim \beta_{\text{sh}}^{-2}y/(1 + y^2)$, and y is limited from kinetic theory and isotropy requirements by $y < \beta_{\text{sh}}^{-1}$ [79]. In relativistic shocks, $\beta_{\text{sh}} \simeq 1$, this leads to $\theta_{\text{F}} \sim 1$, which is essentially confirmed by numerical simulations for both parallel and oblique shocks [80,81].

The time scale for second order Fermi acceleration is given by [31]

$$t_{\text{acc}} \approx \frac{3cr_{\text{L}}}{v_{\text{A}}^2} \left(\frac{\delta B}{B} \right)^{-2} \quad . \quad (\text{C0b})$$

where v_{A} is the Alfvén speed in the plasma. Introducing $y = (B/\delta B)^2$ as above, this yields $t_{\text{acc}} \sim y\beta_{\text{A}}^{-2}t_{\text{L}}$, with $\beta_{\text{A}} = v_{\text{A}}/c$. The condition for efficient scattering of the particles is $\beta_{\text{A}}^2 \ll y$ [30], which directly translates to $\theta_{\text{F}} \sim y\beta_{\text{A}}^{-2} \gg 1$ for second order Fermi acceleration.

Hence, $t_{\text{acc}} \sim t_{\text{L}} = 2\pi r_{\text{L}}/c$ gives a reasonable lower limit for the acceleration time scale of any kind of Fermi acceleration. It may be reached for acceleration in relativistic shock waves; in most cases, however, factors $t_{\text{acc}} \sim 10t_{\text{L}}$ would be more realistic. Throughout the paper, θ_{F} is treated as constant, i.e. which assumes that the diffusion coefficient is proportional to the bohm diffusion coefficient. This is not true in the general case, e.g. for Kolmogoroff turbulence, where $\theta_{\text{F}} \sim 1$ at the maximum energy implies $\theta_{\text{F}} \gg 1$ at lower energies. While this can be important for the comparison of, e.g., electron and proton acceleration time scales [82], it does not affect too much our results near the maximum proton energy.

APPENDIX D: VHE/UHE NEUTRINO EMISSION FROM AGN CORES

The first models which predicted considerable VHE/UHE neutrino fluxes from AGN assumed particle acceleration at shocks in the accretion flow onto the putative central black hole [5,39,6]. By assuming in these models that the power-law 2–10 keV X-ray emission observed from AGN is produced by π^0 -decay from $p\gamma$ and pp interactions, and assuming that the observed diffuse X-ray background is entirely due to AGN, one can estimate the corresponding neutrino flux arising from pp and $p\gamma$ interactions. While the assumption of shocks in the accretion flow near the black hole is more speculative than in jets (unlike the shocks in extended jets, the inner portions of AGN have never been imaged with sufficient angular resolution to infer shocks), core shocks are still the most cited class of models used to estimate expected event rates in neutrino experiments. Thus, it is useful to investigate such models for self-consistency in the face of the pion and muon cooling effects discussed in this paper, which were not considered in the published results (see also more recent papers, e.g. [7,9]).

In principle, we could incorporate these models into our general discussion, because the relevant sizes and time scales in AGN cores are also limited by variability. However, we will not write down here all the observational quantities, but use rather the physical parameters applied in the original papers. The only relevant quantity in the expression of the critical energy for pion and muon cooling (Eqs. (20)) is the value of the magnetic field, since AGN core models are obviously not Doppler boosted (i.e. $\mathcal{D} = 1$). Assuming equipartition of the magnetic field and radiation energy densities, the magnetic field is generally taken as $B \sim [10^3 \text{ G}] \mathcal{L}_{45}^{-1/2}$, where \mathcal{L}_{45} is the UV luminosity of the AGN. (Note that the inverse dependence of the equipartition field on the luminosity arises from the fact that the luminosity scales with the distance of the shock from the Black Hole, and thus with the linear size of the acceleration region, as $\mathcal{L} \propto R$, leading to $u_{\text{ph}} \propto \mathcal{L}^{-1}$.) Applying Eqs. (20) this leads to $\tilde{\mathcal{E}}_{\nu, \text{syn}(\mu)} \sim [10^{16} \text{ eV}] \mathcal{L}_{45}^{1/2}$, and $\tilde{\mathcal{E}}_{\nu, \text{syn}(\pi)} \sim [10^{17} \text{ eV}] \mathcal{L}_{45}^{1/2}$. Disregarding pion and muon cooling, the models of Stecker et al. [5,9] predict a flat single-AGN neutrino power spectrum up to $[2 \times 10^{17} \text{ eV}] \mathcal{L}_{45}^{1/2}$ followed by an exponential cutoff; Protheroe and Szabo [39,7] find essentially the same result. The model of Sikora and Begelman [6] predicts a sharp cutoff at about 10^{15} eV due to their more conservative assumption for the acceleration time scale ($\theta_F \sim 100 \beta_{\text{sh}}^{-2}$, rather than $\theta_F \sim \beta_{\text{sh}}^{-2}$ as assumed in the other models); this is the only model which is not modified by considering pion and muon cooling. For the other models we see that the electron neutrino spectrum and 50% of the muon neutrino spectrum, arising from muon decay, steepen more than one order of magnitude lower in energy than previously assumed.

For the prediction of detector event rates, the integrated diffuse neutrino background contributed by all AGN needs to be considered. Taking simple step functions as approximations for both the steepening induced by muon cooling and the exponential cutoff induced by the maximum proton energy, and noting that the dependence of the maximum energy on the AGN X-ray luminosity remains the same, we can derive a relation which allows to transform the result obtained disregarding muon cooling into the result expected when this effect is considered. The ratio of the integrated neutrino number flux, $\mathcal{F}(\mathcal{E})$, to the unmodified single source spectrum, $f_0(\mathcal{E})$, for \mathcal{E} between the cutoff energies of the least and most luminous AGN, can thus be written as

$$\mathcal{Q}(E) \equiv \frac{\mathcal{F}(\mathcal{E})}{f_0(\mathcal{E})} = \int_{\mathcal{L}_{\min}}^{\mathcal{L}_{\max}} \rho_{\text{AGN}}(\mathcal{L}) \Theta(\hat{\mathcal{E}} \mathcal{L}_{45}^{1/2} - \mathcal{E}) \quad , \quad (\text{D1})$$

where $\rho_{\text{AGN}}(\mathcal{L})$ is the AGN luminosity function. Replacing $\hat{\mathcal{E}} \sim 2 \times 10^{17} \text{ eV}$, as originally assumed, by $\hat{\mathcal{E}}' = 10^{16} \text{ eV}$ as obtained from muon cooling, obviously leads to the relation $\mathcal{Q}'(\mathcal{E}) = \mathcal{Q}(\mathcal{E} \hat{\mathcal{E}} / \hat{\mathcal{E}}') \approx 0.05 \mathcal{Q}(\mathcal{E})$, since $\mathcal{Q} \propto \mathcal{E}^{-1}$ (see original references). Since $\mathcal{Q}'/\mathcal{Q} = \mathcal{F}'/\mathcal{F}$, the diffuse flux of electron neutrinos (as well as muon neutrinos from muon decay) is reduced to about 5% of the value previously obtained, independent of the luminosity function used. Additionally, the exponential cutoff of the diffuse background, corresponding to the cutoff of the most luminous quasars, sets in already below 10^{17} eV rather than at 10^{18} eV . Similarly, the diffuse muon neutrino flux from pion decay is reduced to about 50% of the original value, so that the total VHE muon neutrino flux drops by about a factor of 3 and cuts off at 10^{18} eV .

Clearly, a more detailed calculation is required to obtain reliable flux rates under consideration of detailed spectral modification induced by pion and muon cooling, but our approximate results already show that the effect is important. In particular, we expect no considerable contribution from AGN cores to the electron neutrino spectrum in the energy range interesting for horizontal air shower measurements. No change of the predicted fluxes is expected in the energy range relevant for deep underwater or ice Cherenkov detectors, like Lake Baikal or AMANDA. In the interesting intermediate range, in particular relevant for the event prediction for proposed radio Cherenkov detectors, we obtain a moderately lower flux of muon neutrinos, and a severely reduced contribution of electron neutrinos. Since the model prediction are upper limits (constrained by the diffuse X-ray background), the drop in the rates cannot be balanced by adjusting astrophysical parameters.

- [1] Y. Totsuka, *Rep. Prog. Phys.* **55**, 377 (1992).
- [2] T. Gaisser, F. Halzen, and T. Stanev, *Phys. Rep.* **258**, 173 (1995).
- [3] E. Zas, in *Very High Energy Phenomena in the Universe, 32nd Rencontres de Moriond, Les Arcs, Jan 18-25, 1997* (Editions Frontières, Gif-sur-Yvette Cedex, France, in press), astro-ph/9704016.
- [4] G. Sigl, S. Lee, D. Schramm, and P. Coppi, *Phys. Lett. B* **392**, 129 (1997).
- [5] F. Stecker, C. Done, M. Salamon, and P. Sommers, *Phys. Rev. Lett.* **66**, 2697 (1991), erratum: *Phys. Rev. Lett.* **69**, 2738.
- [6] M. Sikora and M. Begelman, in *High Energy Neutrino Astrophysics*, edited by V. J. Stenger, J. G. Learned, S. Pakvasa, and X. Tata (World Scientific, Singapore, 1992), pp. 114–129.
- [7] A. P. Szabo and R. J. Protheroe, *Astropart. Phys.* **2**, 375 (1994).
- [8] K. Mannheim, *Astropart. Phys.* **3**, 295 (1995).
- [9] F. W. Stecker and M. H. Salamon, *Space Sci. Rev.* **75**, 341 (1996).
- [10] F. Halzen and E. Zas, *ApJ* **488**, 669 (1997).
- [11] G. Parente and E. Zas, in *Procs 7th Int. Symp. on Neutrino Telescopes, Venice, Feb. 1996*, edited by M. Baldo-Ceolin (Dept. Physics, Univ. of Padua, Italy, 1996), p. 345, astro-ph/9606091.
- [12] B. Paczyński and G. Xu, *ApJ* **427**, 708 (1994).
- [13] E. Waxman and J. Bahcall, *Phys. Rev. Lett.* **78**, 2292 (1997).
- [14] J. E. McErny *et al.*, TeV Observations of the Variability and Spectrum of Markarian 421, 25th Int. Cosmic Ray Conference, Durban, 1997, astro-ph/9706125.
- [15] R. J. Protheroe *et al.*, Very High Energy Gamma Rays from Markarian 501, 25th Int. Cosmic Ray Conference, Durban, 1997, astro-ph/9706125.
- [16] K. Mannheim, *A&A* **269**, 67 (1993).
- [17] K. Mannheim, *Space Sci. Rev.* **75**, 331 (1996).
- [18] M. Sikora, G. Madejski, and M. Begelman, in *Relativistic Jets in AGN, Procs., Cracow, 27–30 May, 1997*, edited by M. Ostrowski *et al.* (PUBLISHER, ADDRESS, in press), astro-ph/9708261.
- [19] P. Mészáros and M. J. Rees, *ApJ* **482**, L29 (1997).
- [20] P. L. Biermann, *J. Phys.* **G23**, 1 (1997).
- [21] G. R. Blumenthal and R. J. Gould, *Rev. Mod. Phys.* **42**, 237 (1970).
- [22] K. Mannheim, W. M. Krülls, and P. L. Biermann, *A&A* **251**, 723 (1991).
- [23] J. Jackson, *Classical Electrodynamics*, 2nd ed. (John Wiley & Sons, Inc., New York, 1975).
- [24] M. J. Rees, *MNRAS* **184**, 61P (1978).
- [25] M. J. Rees and P. Mészáros, *ApJ* **430**, L93 (1994).
- [26] R. Sari and T. Piran, *ApJ* **455**, L143 (1995).
- [27] R. D. Blandford and C. F. McKee, *Phys. Fluids* **19**, 1130 (1976).
- [28] E. Fermi, *Phys. Rev.* **75**, 1169 (1949).
- [29] L. Drury, *Rep. Prog. Phys.* **46**, 973 (1983).
- [30] D. B. Melrose, *Plasma Astrophysics: Nonthermal Processes in Diffuse Magnetized Plasmas* (Gordon & Breach, New York, 1980), Vol. II.
- [31] R. M. Kulsrud, in *Particle Acceleration Mechanisms in Astrophysics*, No. 56 in *AIP Conference Procs.*, edited by J. Arons, C. Max, and C. McKee (American Institute of Physics, New York, 1979), pp. 13–26.
- [32] W. M. Krülls, *A&A* **260**, 49 (1992).
- [33] M. Sikora, M. C. Begelman, and M. J. Rees, *ApJ* **421**, 153 (1994).
- [34] B. Rudak and P. Mészáros, *ApJ* **383**, 269 (1991).
- [35] E. Zas, F. Halzen, and R. Vázquez, *Astropart. Phys.* **1**, 297 (1993).
- [36] Particle Data Group, *Phys. Rev. D* **54**, 1 (1996).
- [37] G. M. Webb, L. O. Drury, and P. Biermann, *A&A* **137**, 185 (1984).
- [38] W. Krülls and A. Achterberg, *A&A* **286**, 314 (1994).
- [39] R. J. Protheroe and A. P. Szabo, *Phys. Rev. Lett.* **69**, 2885 (1992).
- [40] K. Mannheim, T. Stanev, and P. L. Biermann, *A&A* **260**, L1 (1992).
- [41] M. Catanese *et al.*, *ApJ* **487**, L143 (1997).
- [42] E. Pian *et al.*, *ApJ* (1997, in press), astro-ph/9710331.
- [43] A. Mastichiadis and J. G. Kirk, *A&A* **320**, 19 (1997).
- [44] K. Mannheim, in *Very High Energy Phenomena in the Universe, 32nd Rencontres de Moriond, Les Arcs, Jan 18-25, 1997* (Editions Frontières, Gif-sur-Yvette Cedex, France, in press), astro-ph/9703184.
- [45] W. Bednarek, Production of Gamma-rays in Blazars, *Procs. Frascati Workshop*, 1997, Mem. S. A. Italy, in press, astro-ph/9711189.
- [46] K. Mannheim, *Science* **279**, 684 (1998).
- [47] E. J. Guerra and R. A. Daly, *ApJ* **491**, 483 (1997).
- [48] C. M. Urry and P. Padovani, *PASP* **107**, 803 (1995).
- [49] K. Mannheim, in *Procs. Heidelberg Workshop on Gamma Ray Emitting AGN, 16–18 Oct, 1996*, edited by J. G. Kirk, M. Camenzind, C. von Montigny, and S. Wagner (MPI Kernphysik, Heidelberg, Germany, 1996), astro-ph/9612066.
- [50] L. M. J. Brown *et al.*, *ApJ* **340**, 129 (1989).
- [51] G. Miley, *ARA&A* **18**, 165 (1980).

[52] P. Grandi *et al.*, *Advances in Space Research* **15**, 23 (1995).

[53] J. A. Gaidos *et al.*, *Nature* **383**, 319 (1996).

[54] J. H. Buckley *et al.*, *ApJ* **472**, L9 (1996).

[55] G. Lamer and S. Wagner, *A&A* (1998, in press), astro-ph/9801007.

[56] T. Takahashi *et al.*, *ApJ* **470**, L89 (1996).

[57] A. Celotti, A. C. Fabian, and M. J. Rees, *MNRAS* (1997, in press), astro-ph/9707131.

[58] C. Thompson, *MNRAS* **270**, 480+ (1994).

[59] M. Schubnell, in *Proc. 4th Compton Symposium, Williamsburg, VA, 1997* (AIP, ADDRESS, in press), astro-ph/9707047.

[60] G. J. Fishman and C. A. Meegan, *ARA&A* **33**, 415 (1995).

[61] P. Mészáros, in *Gamma-Ray Bursts, Procs. 4th Huntsville Symposium, Sep 15–20, 1997, AIP Conference Procs.*, edited by C. A. Meegan, R. Preece, and T. Koshut. (American Institute of Physics, New York, in press), astro-ph/9711354.

[62] C. Kouveliotou, *Science* **277**, 1257 (1997).

[63] P. Mészáros, in *17th Texas Symposium on Relativistic Astrophysics and Cosmology*, Vol. 759 of *Ann. N. Y. Acad. Sci.*, edited by H. Böhringer, G. E. Morfill, and J. E. Trümper (The New York Academy of Sciences, New York, 1995), p. 440.

[64] E. Waxman, *Phys. Rev. Lett.* **75**, 386 (1995).

[65] P. Mészáros and M. J. Rees, *ApJ* **405**, 278 (1993).

[66] J. P. Rachen and P. Mészáros, in *Gamma-Ray Bursts, Procs. 4th Huntsville Symposium, Sep 15–20, 1997, AIP Conference Procs.*, edited by C. A. Meegan, R. Preece, and T. Koshut. (American Institute of Physics, New York, in press).

[67] M. Vietri, *ApJ* **453**, 883 (1995).

[68] F. W. Stecker, *ApJ* **228**, 919 (1979).

[69] J. P. Rachen, Ph.D. thesis, University of Bonn, 1996, <http://www.astro.psu.edu/users/jorg/PhD>.

[70] F. Halzen, The AMANDA Neutrino Telescope: Science Prospects and Performance at First Light, MADPH-97-1007, University of Wisconsin, 1997, astro-ph/9707289.

[71] F. Halzen, Status of Neutrino Astronomy: The Quest for Kilometer-Scale Instruments, MADPH-96-981, University of Wisconsin, 1996, astro-ph/9701029.

[72] G. Fricter, J. Ralston, and D. McKay, *Phys. Rev. D* **53**, 1684 (1994).

[73] A. Butkevitch *et al.*, in *Particles and Cosmology*, edited by E. Alexeev, K. N. V.A. Metveev, and V. Rubakov (World Scientific, Singapore, 1996), pp. 306–315.

[74] A. Nicolaïdis and A. Taramopoulos, *Physics Letters B* **386**, 211 (1996).

[75] T. Abu-Zayyad *et al.*, in *Physics with HiRes Stage 0.5 and Stage 2* (PUBLISHER, ADDRESS, YEAR), oG 10.6.1.

[76] S. Aiso *et al.*, in *The Telescope Array Project* (PUBLISHER, ADDRESS, YEAR), oG 10.6.15.

[77] M. Boratav, *Nucl. Phys. B Procs. Supplement* **48**, 488 (1996).

[78] R. Gandhi, C. Quigg, M. H. Reno, and I. Sarcevic, *Astropart. Phys.* **5**, 81 (1996).

[79] J. Jokipii, *ApJ* **313**, 842 (1987).

[80] D. C. Ellison, F. C. Jones, and S. P. Reynolds, *ApJ* **360**, 702 (1990).

[81] J. Bednarz and M. Ostrowski, *MNRAS* **283**, 447 (1996).

[82] P. L. Biermann and P. A. Strittmatter, *ApJ* **322**, 643 (1987).